ELSEVIER

Marine Geology 133 (1996) 123–156

MARINE GEOLOGY
INTERNATIONAL JOURNAL OF MARINE GEOLOGY, GEOCHEMISTRY AND GEOPHYSICS

Late Quaternary sedimentation and glacial history of the western Svalbard continental margin

Espen S. Andersen [a,1], Trond M. Dokken [b], Anders Elverhøi [a], Anders Solheim [c], Ingrid Fossen [a]

[a] *University of Oslo, Department of Geology, P.O. Box 1047 Blindern, N-0316 Oslo, Norway*
[b] *University of Tromsø, Institute of Biology and Geology, N-9037 Tromsø, Norway*
[c] *Norwegian Polar Institute, P.O. Box 5072 Majorstua, N-0301 Oslo, Norway*

Received 19 October 1995; accepted 14 March 1996

Abstract

Glacigenic sediments recovered in shallow cores from the western Svalbard continental slope, are subdivided into five facies associations based on grain-size, sedimentary structure, mineralogy, petrography and geochemistry. Two diamicton facies are recognised, one of which is interpreted as hemipelagic mud with variable amounts of ice-rafted debris (IRD), and the other as a product of mass-movement. The diamictons are associated with melting of icebergs during glacial melt events and debris flow deposition on the submarine fans during peak glaciation, respectively. Laminated-to-layered mud and turbidites seem to be closely related to eustatic fall in sea level and erosion of banks located on the continental shelf, resulting in accumulation of fine-grained organic-rich deposits and thin silt- and sand layers on the continental slope.

Middle Weichselian was characterised by several phases of extensive iceberg production and input of IRD. The first phase (60–55 ka) is correlated with a glacier advance on Svalbard, but the following phases (54–~44 ka) can not be correlated with glacier advances on land. This demonstrates that there may have been more glaciations than recorded on Svalbard, and that ice sheets at high northern latitudes fluctuated more frequently than previously assumed. The composition of the IRD deposited after 54 ka, suggests that the ice sheets during these advances were located in the eastern Svalbard–Barents Sea area.

The Late Weichselian growth of the Svalbard–Barents Sea Ice Sheet occurred probably in two steps; Nucleation of a continental-based ice sheet between 27 and 22.5 ka, followed by a rapid advance to the shelf edge when the ice margin reached the soft, clay-rich sediments on the continental shelf. Eustatic lowering of the sea level during the initial phase led to bank exposure and erosion, bringing large quantities of fine-grained, organic-rich sediments to the deep-sea. During peak glaciation, glaciers provided a localised supply of sediments to the shelf troughs and the upper slope, which were redistributed by debris flows. The marine-based Svalbard–Barents Sea Ice Sheet started to retreat around 14.5 ka through massive iceberg discharge. The retreat was interrupted by a short-lived advance, accompanied by erosion of the shelf banks and redistribution of organic-rich sediments to the continental slope. The final ice recession started around 12 ka and ended close to 9 ka, when the fjords of Svalbard were essentially ice-free. Large amounts of meltwater released during the removal of the Svalbard–Barents Sea Ice Sheet, cooled down the surface

[1] Present address: Norsk Hydro a.s., P.O. Box 200, N–1321 Stabekk, Norway.

0025-3227/96/$15.00 © 1996 Elsevier Science B.V. All rights reserved
PII S0025-3227(96)00022-9

waters of the Norwegian–Greenland Sea and formed a widespread sea-ice cover between 12 and 8 ka. Input of terrigenous material was greatly reduced during the early part of Holocene. The present interglacial is characterised by erosion of the shelf and upper slope by bottom currents, leaving a prominent lag deposit.

1. Introduction

The number and extent of glaciations on Svalbard during the Weichselian has been extensively discussed during the last 5–10 years. Data from north-western Spitsbergen (Miller et al., 1989), seem to indicate that only an Early Weichselian glaciation (during Isotope Stage 5) reached the continental shelf, and that the ice did not advance beyond the west coast of Spitsbergen during the Middle and Late Weichselian. However, Mangerud and Svendsen (1992) and Landvik et al. (1992) identified three glacial–deglacial cycles of Weichselian age based on studies of beach sections in the inner fjords of Svalbard and near the west coast of Spitsbergen, respectively, and Mangerud and Svendsen (1992) suggest that the ice reached the continental shelf at least during the two latest events. Corresponding dropstone peaks in deep-sea cores from the Fram Strait (Hebbeln, 1992), and studies of cores and shallow seismic data from the continental shelf (Svendsen et al., 1992) support this idea.

This study is based on a number of piston cores ($\leq$8.6 m long) from the continental slope (hereafter referred to as *the slope*) off western Svalbard (Fig. 1). The western margin of Svalbard is characterised by large submarine fans, deposited in front of relatively large troughs which traverse the continental shelf (hereafter referred to as *the shelf*). The troughs form continuations of the fjords of Svalbard, and probably acted as main transport routes for both ice and glacigenic sediments during glaciations (Andersen et al., 1994). The cores used in this study are widely distributed over the study area that includes the Isfjorden and Bellsund fans as well as the slope between them.

The use of sediment cores from continental margins may have advantages over deep-sea cores. Firstly, because a higher sedimentation rate both increases the temporal resolution of the cores and decreases the impact of bioturbation; and secondly, because slopes on high-latitude margins are closer to former ice sheets and therefore will mainly record signals that relate to the evolution of single ice sheets, rather than the less specific signals obtained from deep-sea cores. A great disadvantage is, of course, the risk of obtaining disturbed and discontinuous records due to gravity flows (debris flows and turbidity currents) that are frequent on slopes.

The main objective of this paper is to contribute to the understanding of the glacial development of western Svalbard during the last glacial–interglacial cycle and hence shed more light on the glacial evolution of the entire Svalbard–Barents Sea area. The stratigraphic framework of the slope and shelf sediments, and the palaeoceanographic evolution during the Late Quaternary are well established (Hebbeln et al., 1994; Dokken, 1995; Elverhøi et al., 1995a). However, the glacial history of the Svalbard and Barents Sea areas is still not fully understood. In this paper, we will combine the chronostratigraphic framework with sedimentary facies associations in order to establish a better understanding of the phases during the final build-up and the subsequent recession of the Svalbard–Barents Sea Ice Sheet. In addition, the paper present new information about slope processes that are taking place close to a large marine-based ice sheet.

2. Physiography and hydrography

The western Svalbard shelf is 60–85 km wide with water depth ranging from 400 m to less than

Fig. 1. A. Map showing the study area at the western Svalbard margin. Bathymetry is shown in 100 m and 500 m contours above and below 1000 m, respectively. Filled dots with numbers refer to core sites, and heavy lines with numbers refer to figures shown in the paper. *VMF*= Van Mijenfjorden. B. Index map showing the study area, Svalbard, Greenland, Iceland, Fennoscandia, and the 500 m contour (shelf edge). *SB*= Spitsbergen Bank; *SF*= Storfjorden Fan; *BF*= Bjørnøya Fan; *NGS*= Norwegian–Greenland Sea.

A

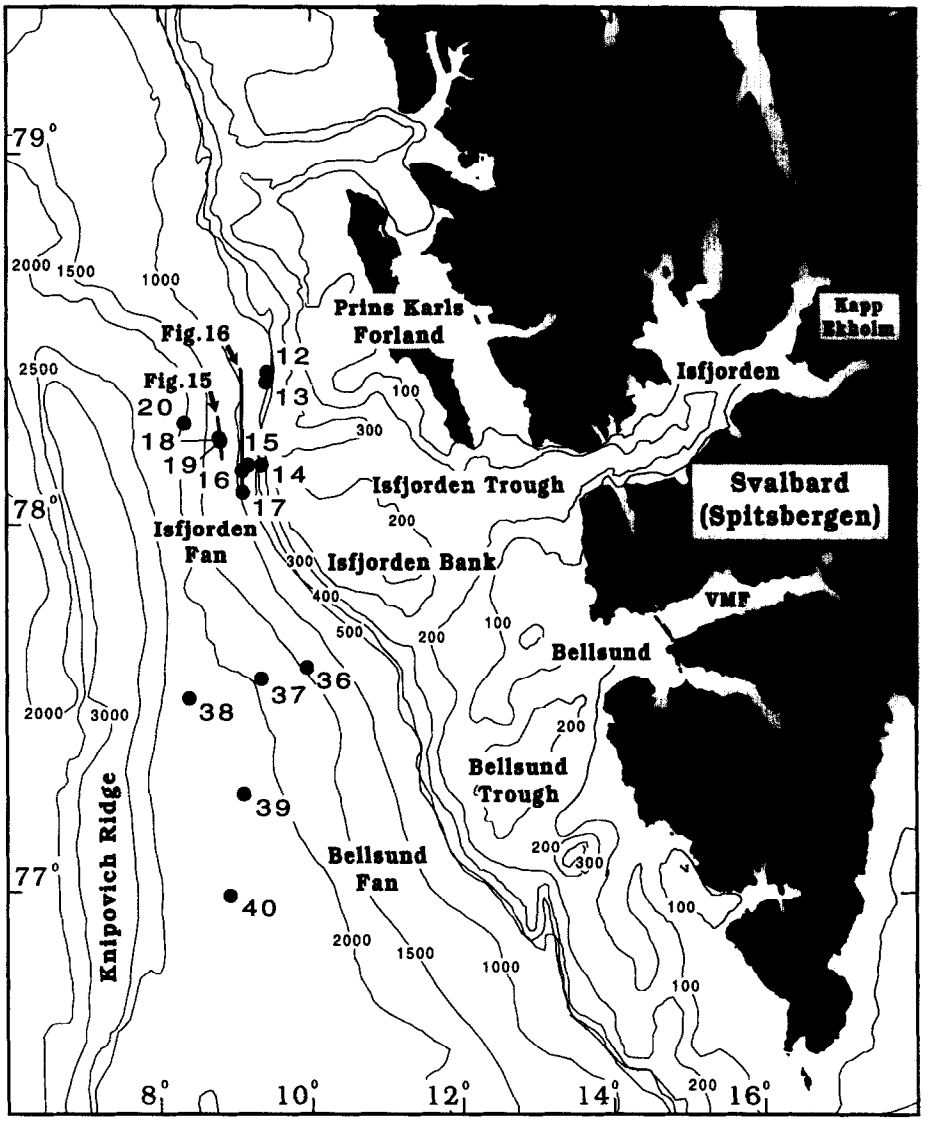
79°
78°
77°
8°
10°
12°
14°
16°
2000
1500
1000
2500
100
300
200
400
500
3000
Prins Karls Forland
Kapp Ekholm
Isfjorden
Svalbard (Spitsbergen)
Isfjorden Trough
Isfjorden Bank
Isfjorden Fan
VMF
Bellsund
Bellsund Trough
Bellsund Fan
Knipovich Ridge
Fig.16
Fig.15
12
13
14
15
16
17
18
19
20
36
37
38
39
40

B

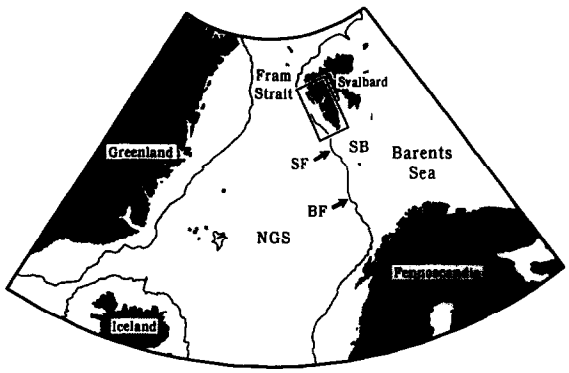
Fram Strait
Svalbard
Greenland
SF
SB
Barents Sea
BF
NGS
Iceland

100 m (Fig. 1). The shelf is characterised by shallow banks and glacially eroded troughs (Boulton, 1990). The troughs are associated with large submarine fans, of which the Isfjorden Fan is the largest. The close relationship between the fjords, the shelf-troughs and the submarine fans indicates a higher degree of sediment transport through the troughs compared to the areas in between. The slope is steep with a gradient of up to 5° (Andersen et al., 1994). The Knipovich Ridge spreading axis is located near the western margin of Svalbard, and the Isfjorden Fan has prograded into the axial valley (Fig. 1).

The present hydrography is influenced by both the West Spitsbergen Current (Aagaard et al., 1985), which supplies Atlantic water to the shelf area, and highly saline cold bottom water coming from the Storfjorden area (Anderson et al., 1988). Guided by topography and earth rotation, this bottom water flows around the southern tip of Svalbard into the Fram Strait and sinks to depths of more than 2000 m (Quadfasel et al., 1988). The shelf area, especially the outer part, tends to be one of sediment reworking (Boulton, 1990), erosion of earlier sediments and the formation of sandy and gravely lag horizons (Solheim et al., 1991). This is caused by the long-shelf geostrophic current and upwelling of deep water.

The study area lies oceanward of a fjord system occupied by former glaciers in western Svalbard (Landvik et al., 1992; Mangerud et al., 1992; Mangerud and Svendsen, 1992; Svendsen et al., 1992). These glaciers drained a large part of the Svalbard Ice Sheet, and followed the line of Isfjorden and Van Mijenfjorden. The configuration of the ice-drainage basin is thought to have remained relatively constant during the late Quaternary. Therefore, the margin sediments should reflect all stages of the last Svalbard glaciation.

3. Material and methods

A high number of shallow cores (0.2–8.6 m long) were recovered from the western Svalbard margin on board *M/S Håkon Mosby* in 1990 (Solheim et al., 1991). The core selection of this study consists of 25 box-, gravity- and piston-cores (Fig. 1, Table 1). The cores were split and described, and samples were collected for geotech-

Table 1
Core selection and core locations

Core	Type	Latitude	Longitude	WD(m)
NP90-12A	BC	78°24.46'N	9°24.9'E	690
NP90-12B	PGC	78°24.47'N	9°24.87'E	683
NP90-12C	PC	78°24.47'N	9°24.88'E	628
NP90-13A	PGC	78°22.84'N	9°23.84'E	696
NP90-13B	GC	78°22.23'N	9°23.95'E	691
NP90-14	GC	78°10.03'N	9°20.84'E	486
NP90-15	BC	78°9.97'N	9°10.07'E	596
NP90-16	GC	78°9.76'N	9°5.68'E	974
NP90-17	GC	78°9.09'N	9°5.58'E	976
NP90-18A	BC	78°14.18'N	8°47.79'E	1444
NP90-18B	GC	78°14.18'N	8°47.73'E	1446
NP90-18C	PC	78°14.18'N	8°47.82E	1444
NP90-19A	GC	78°13.7'N	8°48.29'E	1431
NP90-19B	PC	78°13.7'N	8°48.17'E	1427
NP90-20A	BC	78°16.09'N	8°20.06'E	2070
NP90-20B	PC	78°16.15'N	8°19.73'E	2074
NP90-36A	BC	77°37.03'N	9°56.23'E	1360
NP90-36B	PGC	77°37.04'N	9°56.18'E	1360
NP90-37	BC	77°35.13'N	9°19.55'E	1800
NP90-38A	BC	77°31.35'N	8°23.24'E	2327
NP90-38B	PGC	77°31.1'N	8°24.02'E	2326
NP90-38C	PC	77°31.54'N	8°23.04'E	2328
NP90-39	PC	77°15.49'N	9°5.58'E	2119
NP90-40A	BC	76°58.2'N	8°54.58'E	2255
NP90-40B	PC	76°58.28'N	8°54.54'E	2254

WD = water depth; BC = box core; PGC = plastic gravity core; GC = gravity core; PC = Piston core. The suffix of the core number refers to site number in Fig. 1.

Table 2
Analyses procedures for XRD

Trace	°2Θ	PTH (°C)	Period (hrs)	Sample type	Detection of
U	2–50	–	–	bulk and clay	–
SSC	26–28.5	–	–	bulk	KF and P
SSC	24–28.5	–	–	clay	CH and KA
EG	2–50	60	24	clay	EM
H	2–50	550	2	clay	EM, CH and KA

U = untreated, SSC = slow scan, EG = ethylene glycol: H = heating, PTH = Pre-treatment heating, KF = K-feldspar, P = plagioclase, CH = chlorite, KA = kaolinite, EM = expandable minerals.

Table 3
Identified minerals in the slope sediments

Minerals	Peak position in degrees 2θ(Cu Kα radiation)	d values (Å)	Intensity factors (Schültz, 1964)
Amphiboles	10.4–10.8	8.2–8.5	–
Clay minerals	19.9	4.46	100
Quartz	26.6	3.35	2000
K-feldspar	27.5	3.24	1000
Plagioclase	28.0	3.19	1000
Calcite	29.4	3.03	1000
Dolomite	31.0	2.88	1000
Siderite	31.7–31.9	2.81–2.82	600
Pyrite	33.1	2.71	250

nical, mineralogical, geochemical and grain-size analyses. X-radiographs were made from split cores to observe sedimentary and biogenic structures. Measurements of physical properties included water content (percent of wet weight), porosity, wet bulk density, dry bulk density, undrained shear strength and compressional-(p)-wave velocity.

Both unoriented crushed whole-rock samples and specimens of mg-saturated clays (<2 μm) were prepared for XRD analyses. The analyses were run according to Andersen et al. (1995). Five XRD traces were run for each sample (Table 2). Semi-quantitative mineral abundances were estimated from diffractograms of whole-rock samples using the intensity factors (Table 3) of Schültz (1964), and clay mineral abundance estimates were derived from the oriented specimen diffractograms. Chlorite (004)/kaolinite (002) peak height ratio was used to determine the chlorite-to-kaolinite weight ratio using the method described by Rundberg (1989):

$$\mathrm{ch/ka_{weight}} = (\mathrm{ch/ka_{peak}})^2$$

where ch is chlorite and ka is kaolinite. Clay mineral percentages were calculated from peak areas on diffractograms of glycolated specimens corrected as indicated by Pearson and Small (1988) and Pearson (1990), and identified peaks are shown in Table 3. The mineralogical investigations were accompanied by visual determination of the ice-rafted debris (>0.5 mm).

The amount of total carbon (TC) and total organic carbon (TOC) were measured on a LECO 5344 furnace on ground whole rock samples. Pyrolysis was conducted on similar samples, and performed on a Rock Eval II pyrolysis unit with a TOC module. The percentage of carbonate was calculated using the following equation:

$$\mathrm{CaCO_3}(\%) = (TC - TOC) \cdot \frac{Mw_{\mathrm{CaCO_3}}}{Mw_{\mathrm{C}}} = IC \cdot 8.33$$

where Mw is mole weight and IC is inorganic carbon. This is a reasonable assumption, since there is a good agreement between the calcite values obtained from the LECO and XRD runs, with correlation coefficients as high as 0.96. C/N ratios were determined using a Hereaus CHN-O-Rapid elementary analyser at the University of Bremen, Germany. Standard sieves were used to determine the grain size distribution of the coarse fraction (>63 μm), and a SediGraph 5000D particle size analyser (Micromeritics, 1978; Stein, 1985) was used for grain-size measurements of the silt and clay fractions.

The foraminiferal and stable isotope stratigraphy of the cores have been presented in detail by Dokken (1995). Palynological investigations have been carried out on one of the lower slope cores (NP90-39) in order to investigate different source areas (Elverhøi et al., 1995a).

4. Age control

Seventeen AMS ^{14}C dates have been performed on carbonate fossils from cores NP90-12B, -36B and -39 (Dokken, 1995), and NP90-18C. These dates were performed on the planktic foraminifera *Neogloboquadrina pachyderma* (sin.), and approximately 1500–2000 tests were picked out from each sample.

The age model of the slope deposits is based on the radiocarbon datings and oxygen isotope records of *N. pachyderma* (sin.) (Dokken, 1995) (Fig. 2). Additional evidence is provided by the occurrence of the benthic foraminifera *P. bulloides* (Dokken, 1995) characterising the Isotope Stages 5a and 1 (Haake and Pflaumann, 1989).

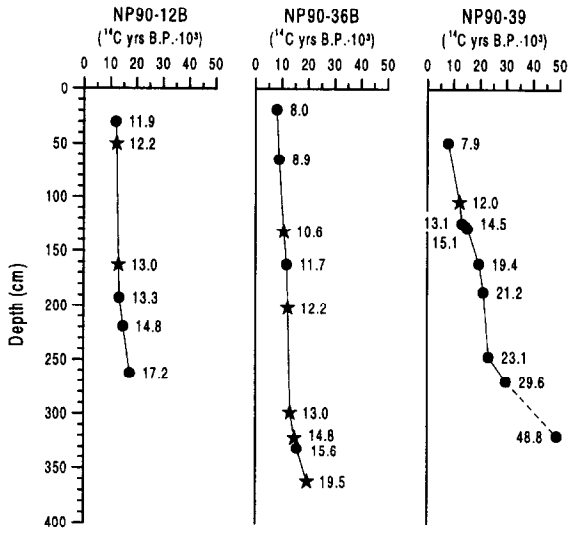

Fig. 2. Radiocarbon ages (filled circles) plotted against depth in three slope cores. Filled stars represent age estimate based on correlation of oxygen isotope records (Dokken, 1995).

The stratigraphy is fairly consistent above T4 (Fig. 4B), spanning the last 40–35 ka. The uncertainties of the chronology below T4 restrict the accuracy with which estimates accumulation rate can be made. Extrapolation of the combined radiocarbon-oxygen isotope records suggest that the records of cores NP90-38C and -39 go back to approximately 135 and 65 ka, respectively, implying average sedimentation rates of 4 cm/ka and 9 cm/ka, respectively. The difference in sedimentation rates is only apparent, since a large, but unknown part of the core sections near T4 probably is missing due to erosion. Two dates are obtained in core NP90-18C at 182.5 cm depth (Fig. 13D), yielding ^{14}C ages of 19,195±225 yr B.P. (Ua-3270) and 19,205±210 yr B.P. (Ua-3271). The ages are normalised to $\delta^{13}C = 0‰$ relative to PDB and corrected for reservoir effect by subtracting 440 yr (Mangerud and Gulliksen, 1975).

5. Results

To aid both the core description and the interpretation of the depositional environment, it should be noted that sites 12, 36 and 37 are located on the upper slope while sites 38, 39 and 40 are located on the lower slope (Fig. 1). The remaining sites (13 to 20) are located on the upper part of Isfjorden Fan. Cores NP90-12B, -36B and -39 are used as references, and the corresponding records will be used for illustrations.

5.1. Physical properties and texture

The physical properties of the slope cores show values typical for normally consolidated sediments (Solheim et al., 1988; Solheim, 1991; Sættem et al., 1992; Andersen et al., 1995) and a gradual downcore effect of increased overburden (Fig. 3). The water content reflect different depositional/erosional developments. In sediments deposited on the lower slope, water content drops from values between 50 and 60% in the top to 30–40% at approximately 80 cm below the seafloor (Fig. 3B). Most of the cores on the upper slope do not record this drop, and the water content of the upper fan cores quickly reaches approximately 20% (Fig. 3A). Undrained shear strength increases from values between 1 and 10 kPa to values about 15 kPa at approximately 250 cm. The values are constant below 250 cm. Wet bulk density is fairly constant throughout the cores with values around 1.5–1.8 g/cm^3. Some of the box cores show lower (1.3–1.5 g/cm^3) values, and the upper fan cores show generally higher (1.8–2 g/cm^3) values. The water and density records suggest that the upper slope cores and the cores obtained from the upper part of Isfjorden Fan may lack the youngest part of the geological record. Compressional wave velocity shows no particular downcore trend, and the high (1200–1800 m/s) variability is most likely a function of low precision during measurements.

There is a reasonably close relationship between the grain-size distribution and physical properties, such as water content and dry bulk density (Fig. 4B). Thus, the fluctuations in physical properties are partly grain-size effects. The major part of the slope sediments are characterised as slightly sandy, silty clay (Fig. 4). Gravel and sand are generally most abundant in the upper part of Isfjorden Fan (Fig. 4C). Sand and silt layers (T1–T4) in the lower slope sediments show up on the grain-size distribution records as distinct peaks

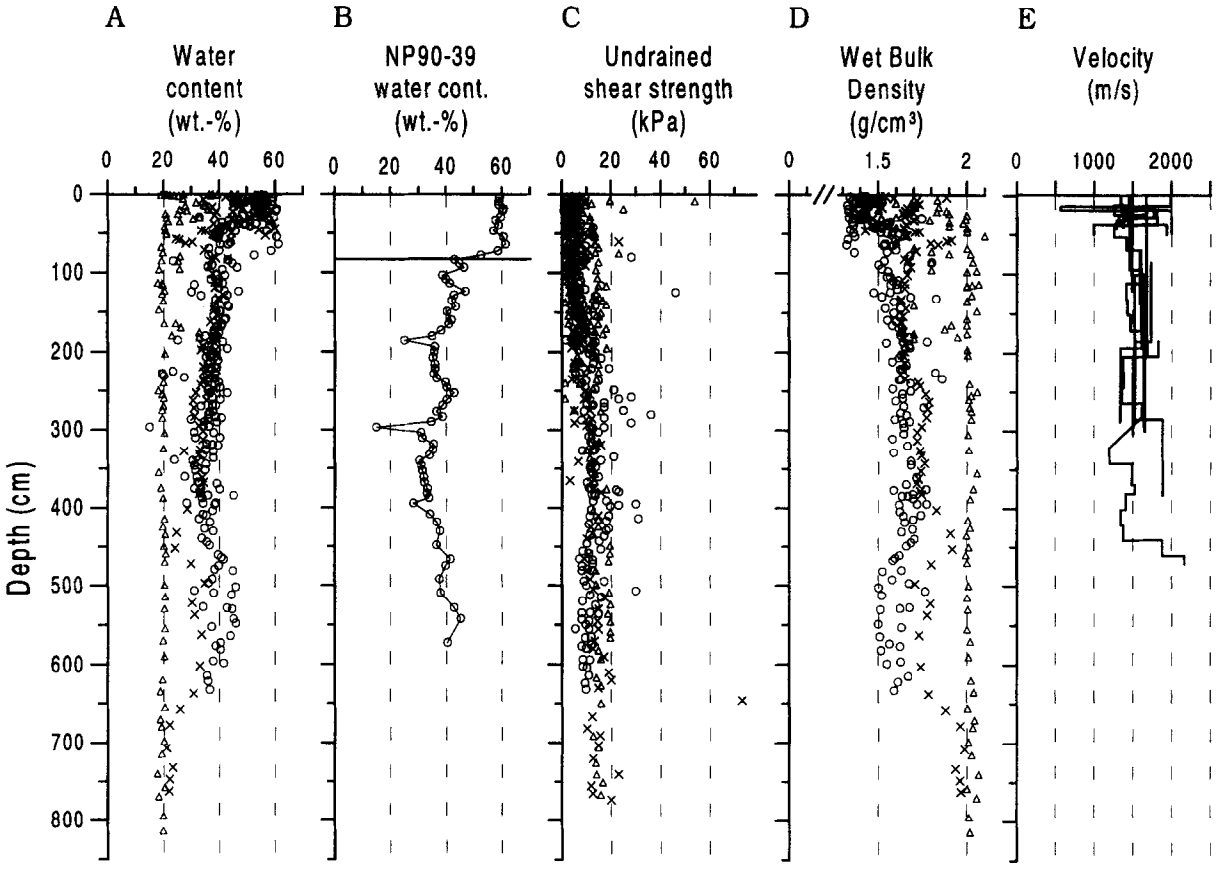

Fig. 3. Composite diagram showing (A) water content, (B) water content in core NP90-39 (lower slope), (C) undrained shear strength, (D) wet bulk density, and (E) compressional-(p)-wave velocity. Open circles: lower slope; crosses: upper slope; open triangles: upper part of Isfjorden Fan.

(Fig. 4B). The lowermost layer (T4) is very sandy and is found in all the lower slope cores. The other layers (T1–T3) are less sorted (Fig. 5) and contain more silt and clay (Fig. 4). The skew-sorting relationship (Fig. 5) suggests that these sand and silt layers were deposited from bottom currents (e.g., turbidity currents).

5.2. *Carbonate and organic carbon*

The content of carbonate and organic carbon is highly variable in the slope sediments (Fig. 6). In addition, there is a strong negative correlation between carbonate and organic carbon, except for the uppermost part of the section where they are positively correlated (Fig. 6B). The lower slope cores contain two zones with relatively high (2.3–12.7%) carbonate and relatively low (0.2–1.1%) organic carbon contents. Only the uppermost zone is recorded in the cores on the upper slope (Fig. 6A). Each of these zones are followed by sections with relatively low (1.5–8.5%) carbonate and high (0.2–2.5%) organic carbon contents. This relationship is not present on the upper part of Isfjorden Fan (Fig. 6C), and below T4 where the $CaCO_3$ content is generally decreasing downcore while the amount of organic carbon is generally increasing, reaching values of up to 2.6% at the bottom of core NP90-39 (Fig. 6B). The $CaCO_3$ content on the upper part of Isfjorden Fan is high, varying between 2 and 17.2%, and the amount of organic carbon varies between 0.3 and 1.5%.

According to Henrich et al. (1989), high organic

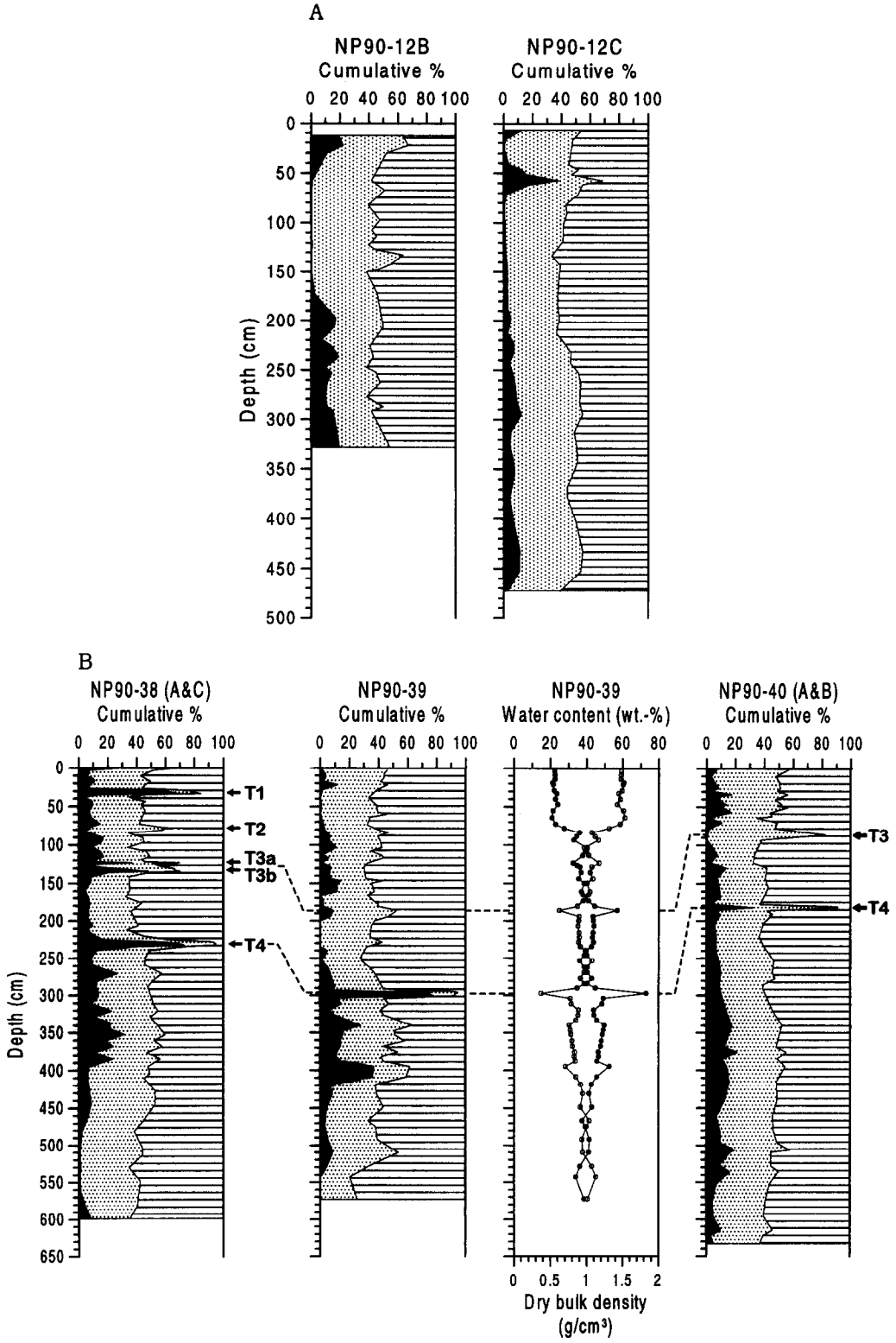
A
NP90-12B
Cumulative %
0 20 40 60 80 100
NP90-12C
Cumulative %
0 20 40 60 80 100
Depth (cm)
0 50 100 150 200 250 300 350 400 450 500
B
NP90-38 (A&C)
Cumulative %
0 20 40 60 80 100
NP90-39
Cumulative %
0 20 40 60 80 100
NP90-39
Water content (wt.-%)
0 20 40 60 80
NP90-40 (A&B)
Cumulative %
0 20 40 60 80 100
T1
T2
T3a
T3b
T4
T3
T4
Depth (cm)
0 50 100 150 200 250 300 350 400 450 500 550 600 650
0 0.5 1 1.5 2
Dry bulk density
(g/cm³)

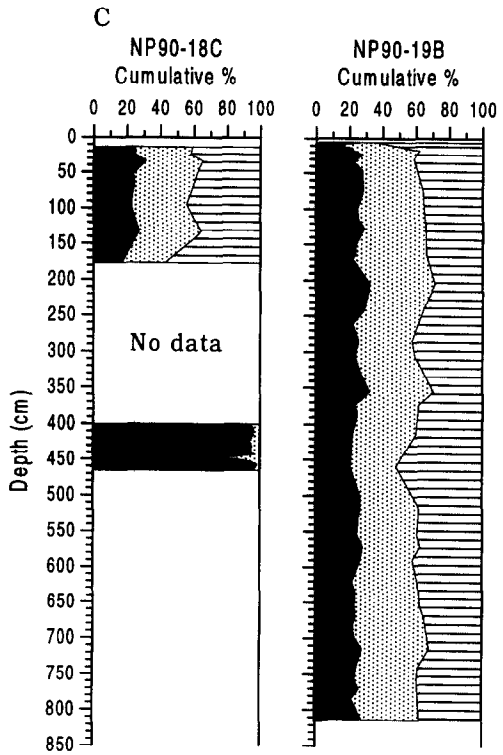

Fig. 4. Grain-size distribution (from left to right: gravel–sand silt–clay) from (A) upper slope, (B) lower slope, and (C) upper part of Isfjorden Fan. The four turbidites identified are marked by *T*1–*T*4. Note the reasonably close relationship between the grain-size distribution, water content (line with open circles), and dry bulk density (line with closed circles) which has been plotted for core NP90-39.

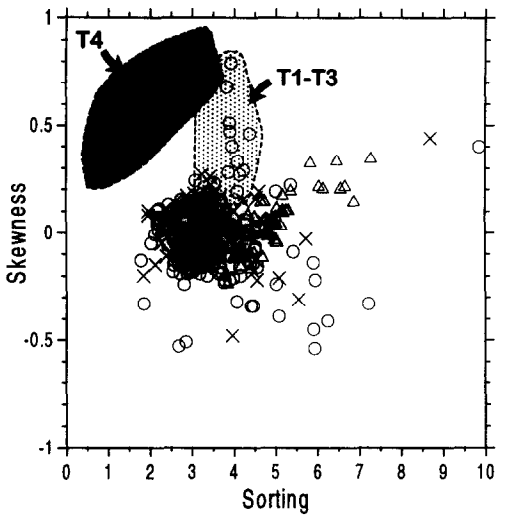

Fig. 5. The skew-sorting plot shows that the slope sediments are relatively poorly sorted with a variable skewness. The turbidite *T*4 is better sorted than the other, more fine-grained turbidites (*T*1–*T*3). Calculations are based on Folk and Ward (1957). See Fig. 3 for symbol explanation.

carbon content in deep-sea sediments should reflect input from erosion of terrigenous organic-rich sediments outcropping on continental shelves, and corresponding low $CaCO_3$ content is probably caused by partial oxidation and decreased deep-water renewal. In addition, Hebbeln et al. (1994) suggest that the $CaCO_3$-rich sections in core NP90-39 (corresponding with high numbers of the planktonic foraminifera species *Globigerina quinqueloba*), can be interpreted as reflecting increased surface water productivity and seasonally open waters.

5.3. Source of the organic material

5.3.1. C/N ratios

The average C/N ratio of the slope deposits is 11.8, with variations from 6.6 to 16.6 (Fig. 7). Stevenson and Cheng (1972) were the first to observe similar irregularities with increasing depth, and they suggest that the fluctuations may be related to alternating warm and cold periods. Therefore, the zones of high C/N ratios coincide with glacial stages and increased input of terrestrial organic matter, and the intervals between these zones may represent interstadial and interglacial periods that were dominated by primary production. Hebbeln et al. (1994) suggest that the high input of fine-grained organic-rich sediments was caused by sweeping-out of shelf and fjord sediments as the glaciers entered the shelf off Svalbard.

5.3.2. Pyrolysis

Downcore variations of free or adsorbed hydrocarbons (S1), hydrocarbons generated by pyrolytic degradation of kerogen (S2), and CO_2 generated (S3) in core NP90-39 show an irregularity in the levels with increasing depth (Fig. 8). The S2 records especially show several peaks. Since the accuracy of T_{max} is about 1–3°C (Peters, 1986), we have chosen to reject T_{max} values for samples with S2 peaks less than 0.2 mg HC/g rock. Hence,

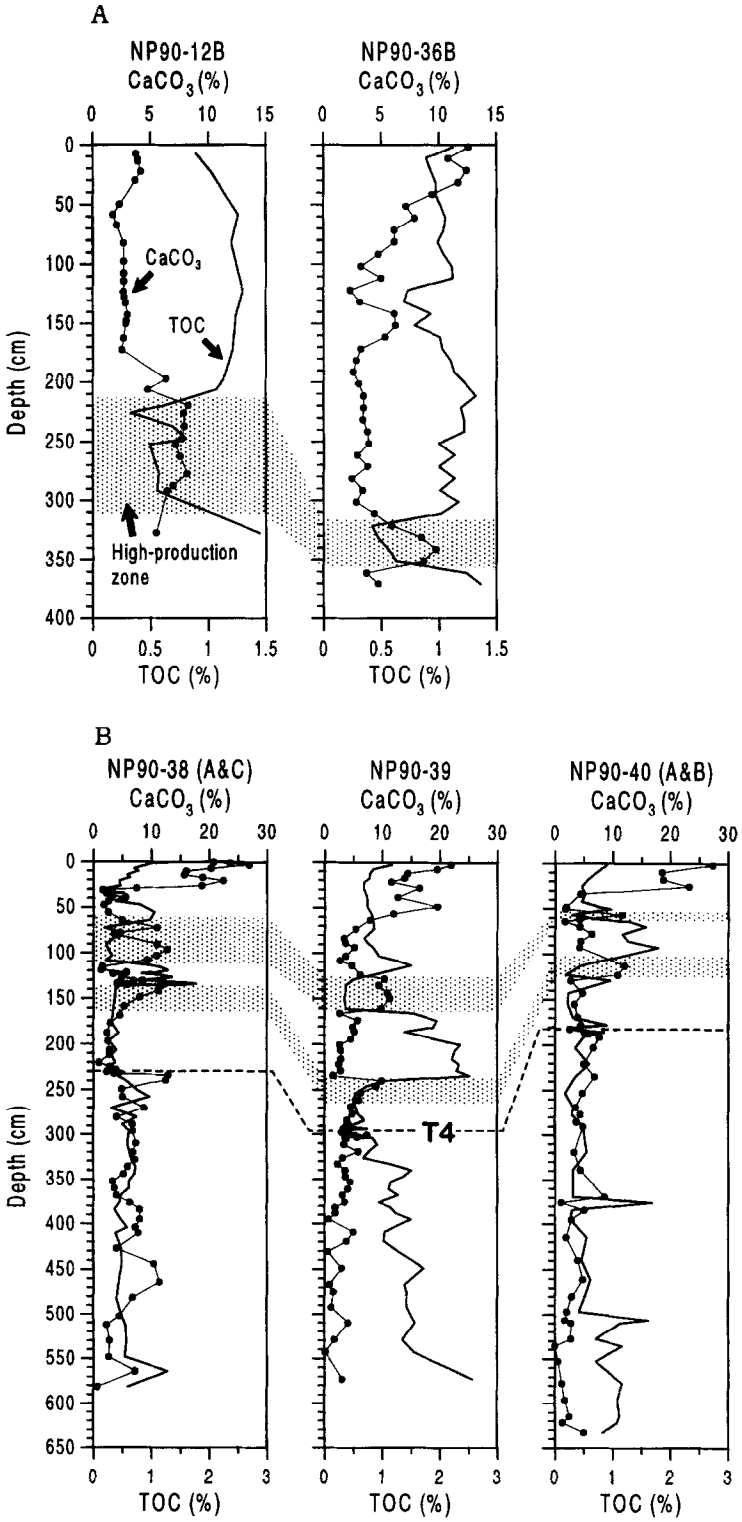
A
NP90-12B
CaCO3 (%)
NP90-36B
CaCO3 (%)
0 5 10 15
CaCO3
TOC
High-production zone
Depth (cm)
0 50 100 150 200 250 300 350 400
0 0.5 1 1.5
TOC (%)
B
NP90-38 (A&C)
CaCO3 (%)
NP90-39
CaCO3 (%)
NP90-40 (A&B)
CaCO3 (%)
0 10 20 30
T4
Depth (cm)
0 50 100 150 200 250 300 350 400 450 500 550 600 650
0 1 2 3
TOC (%)

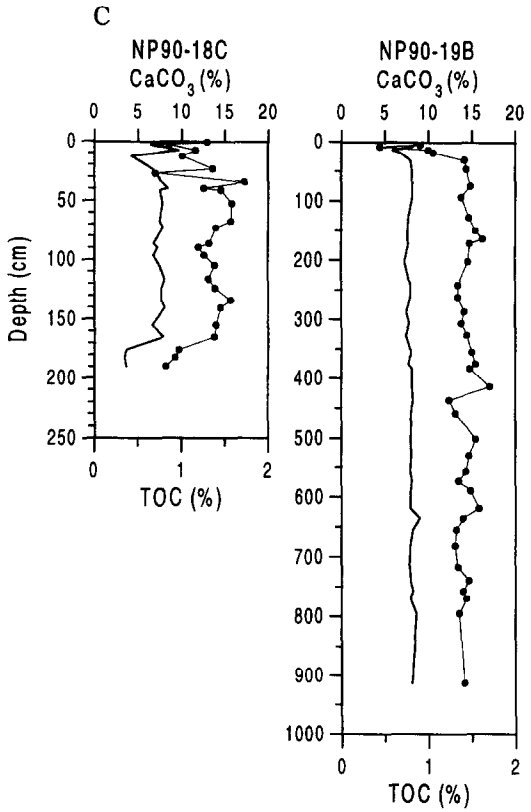

Fig. 6. Downcore variations in $CaCO_3$ (wt.-%) and TOC (wt.-%). (A) Upper slope, (B) lower slope, and (C) upper part of Isfjorden Fan. The high-production zones (high $CaCO_3$ content: rastered) correspond with two periods (27–22.5 ka and 19.5–14.5 ka) with advection of warm Atlantic water to the Norwegian–Greenland Sea (Hebbeln et al., 1994).

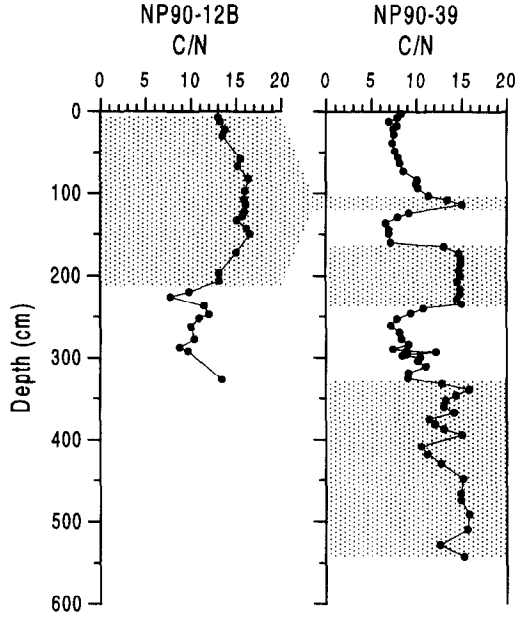

Fig. 7. Downcore variations in C/N ratio in cores NP90-12B (upper slope) and NP90-39. Rastered zones indicate periods with increased input of terrigenous organic-rich material.

we also reject the corresponding hydrogen index (HI) values.

The data distinguishes two modes, one associated with relatively high S2 and T_{max} values, and one with low S2 and high oxygen index (OI) values. It seems obvious that the downcore distribution of organic matter and carbonate has strongly affected the pyrolytic parameters, since higher TOC and $CaCO_3$ samples generate more pyroproducts (S2) and CO_2 (S3), respectively (Fig. 8).

As with the C/N ratios, the results from the pyrolysis show that recycling has dominated the processes on the western Svalbard continental margin. This is expressed by the T_{max} values that are much higher than expected based on the actual maturity of the sediments. It seems clear that most of the organic material associated with high T_{max} values was brought into the basin from the shelf area. A terrestrial origin is suggested by the generally low HI values. Furthermore, the anomalous high OI values indicate extensive oxidation and/or contribution from carbonate present in the cores. In conclusion, the pyrolytic response reflects a cyclic pattern of glacial erosion that has reworked the shelf sediments.

5.4. *Whole-rock and fine-fraction mineralogy*

Vertical profiles through the slope cores (Figs. 9 and 10) show a moderate variation in whole-rock mineralogy. One general feature is the dominance of clay minerals, except in the silty/sandy layers, where quartz dominates. A significant observation in relation to the distribution of interstratified illite–smectite (I–S) concerns the distribution of feldspar. Plagioclase is generally present through all core profiles and varies little in abundance, whereas K-feldspar is relatively abundant except in one particular zone where it is more or less

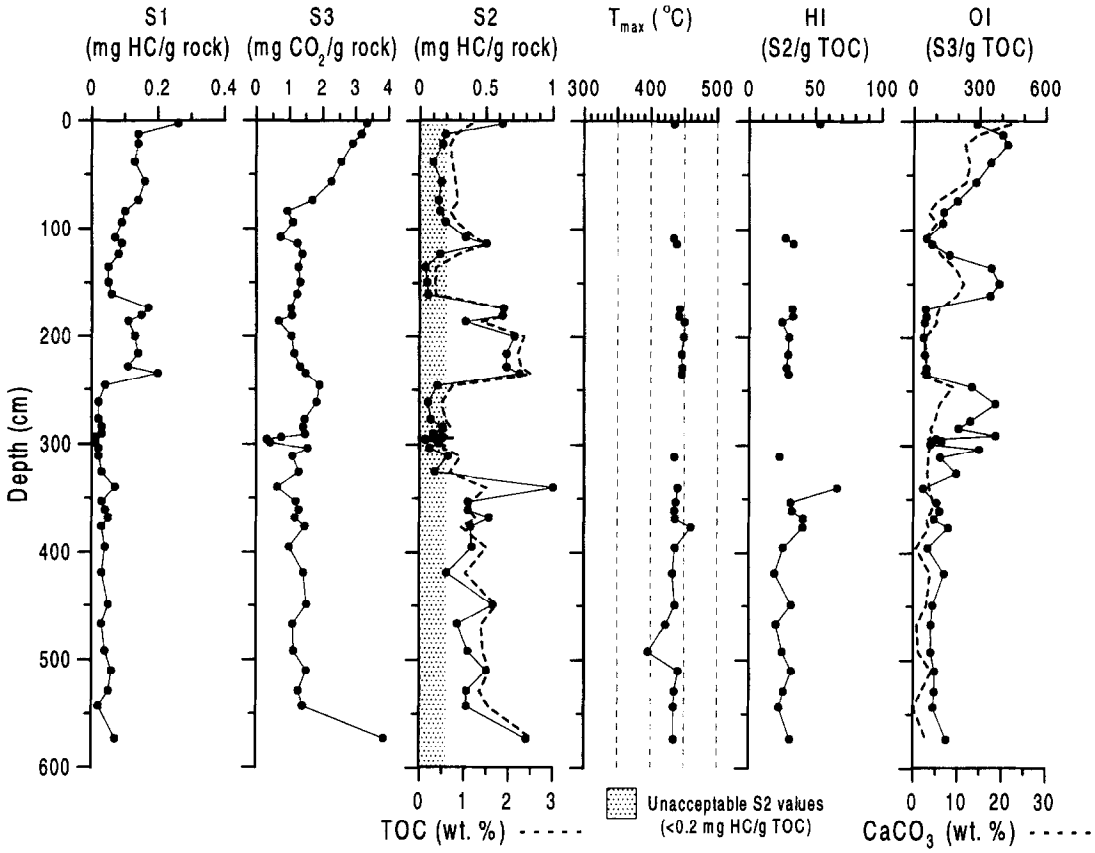

Fig. 8. Geochemical log for whole rock samples from core NP90-39. Anomalous results for $S2$ and T_{max} are due to repeated deposition of allochthonous organic material. The downcore distribution of $CaCO_3$ has strongly affected the oxygen index (OI).

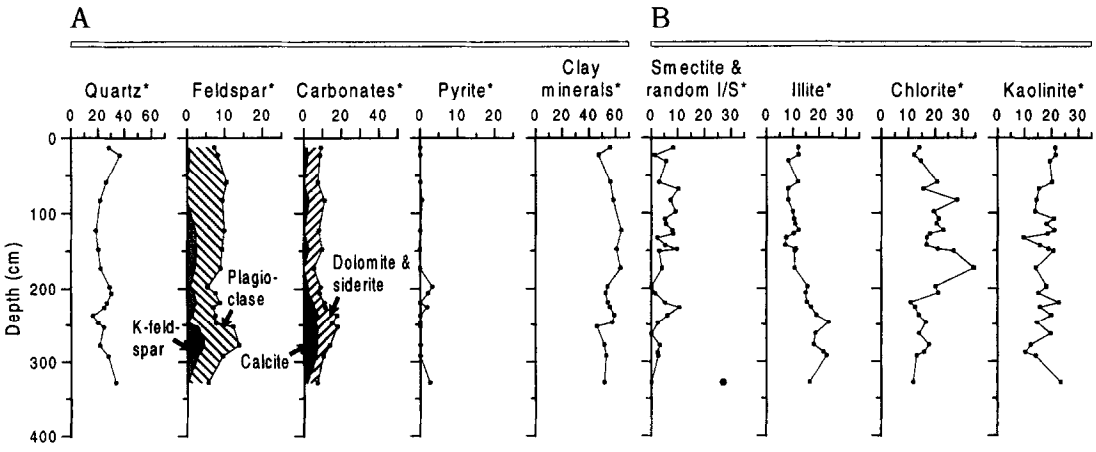

Fig. 9. Relative distribution of minerals in (A) whole rock samples and in (B) the clay size-fraction in core NP90-12B. The bottom sample corresponds with the upper part of the smectite-free zone in core NP90-39 (Fig. 10). Note different horizontal scales. Nomenclature: * = wt.-%, • = ordered I-S.

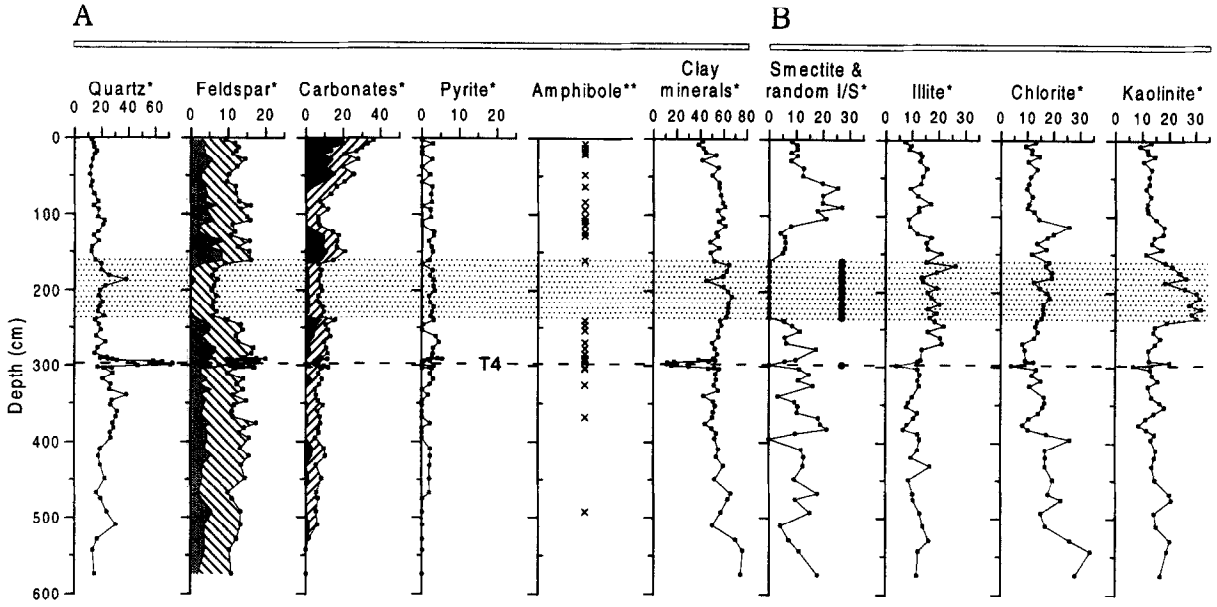

Fig. 10. Relative distribution of minerals in (A) whole rock samples and in (B) the clay size-fraction in core NP90-39. Note different horizontal scales. Nomenclature: * = wt.-%, ** = occurrence, • = ordered I-S. Rastered area marks the zone lacking K-feldspar, smectite and amphibole. Distribution of feldspars and carbonates, see Fig. 9.

absent (Fig. 10). The distribution of calcite reflects the occurrence of planktonic foraminifera in the samples (Hebbeln et al., 1994; Dokken, 1995). Most samples contain some dolomite, but the distribution does not change significantly downcore. Siderite is also present, and highest values are obtained in the uppermost ~50 cm of the cores. The source rocks for siderite are thought to be Jurassic shales from Spitsbergen, which contain abundant siderite concretions and sideritic carbonate lenses (Bjørlykke and Elverhøi, 1975). The presence of amphibole, although in very small concentrations, may be connected with magmatic and especially metamorphic source rocks (Hurlbut and Klein, 1977) and may give further information on transport paths and slope processes.

Despite the general uniformity in whole-rock mineralogy of the samples studied, the profiles of the fine fraction exhibit a great deal of variation (Figs. 9 and 10). Smectite is abundant in most of the samples except in the K-feldspar-poor zone dominated by kaolinite (Fig. 10). The smectite values are generally higher in core NP90-39 than in core NP90-12. The origin of smectite is problematic since in the present-day oceans, it does not reveal a latitudinal distribution pattern as clear as that of the other clay minerals. Smectite is not common on Svalbard (Elverhøi et al., 1989) and probably not in the Spitsbergen Bank area (see later discussion). Kuhlemann et al. (1993) suggest that distribution of smectite in the Norwegian–Greenland Sea is controlled mainly by sea ice transport rather than current transport, and that the main source area is the shelf off Faeroe Islands. Smectite is also a major clay mineral in sediments of the Laptev Sea (Stein et al., 1994a), indicating transport with sea ice through the Arctic Ocean, or via the Barents Sea as also suggested for the north-western Barents Sea (Elverhøi et al., 1989; Forsberg, 1983).

During diagenesis, smectite incorporates potassium to form interstratified illite–smectite (I–S) (Pearson, 1990). Most of the samples in our cores contain detectable amounts of interstratified illite–smectite. For most of the I–S a continental origin is assumed, since it is common on Svalbard (Bjørlykke et al., 1978).

Kaolinite is also abundant through all core profiles, especially in the zones lacking smectite and K-feldspar (Fig. 10). Kaolinite occurring in

polar regions may be derived from weathering of older, kaolinite-bearing sediments and palaeosols, because kaolinite cannot form under glacial conditions (Ehrmann et al., 1992). Kaolinite is common on Svalbard, generated through diagenetic alteration (Elverhøi and Grønlie, 1981). The formation of kaolinite during diagenesis takes place via dilute acidic pore waters reacting with feldspars. High contents of kaolinite probably document the accumulation of physical weathering products of sedimentary rocks located in eastern Svalbard or in the Barents Sea (Sigmond, 1992).

Chlorite is common in the slope sediments off Svalbard (Figs. 9 and 10). It is a characteristic mineral of low-grade, chlorite-bearing metamorphic and basic igneous source rocks, but is not very resistant against weathering and transport (Ehrmann et al., 1992). Thus, it reflects relatively short travel distances. We therefore consider chlorite as detrital, being the product of physical weathering and glacial scour, particularly of crystalline rocks, such as those that are common along the west coast of Spitsbergen and widespread in Scandinavia. The relative strong fluctuations in the chlorite concentration may represent oscillations in the intensity of glaciations on Svalbard and Fennoscandia.

The illite records illustrate only minor long-term changes. Highest concentrations are associated with the smectite-free zone (Fig. 10). In contrast to chlorite, illite tends to be derived from more acidic crystalline rocks, and is relatively resistant (Ehrmann et al., 1992). Furthermore, illite can be transformed from smectite during burial diagenesis in argillaceous sediments if K-feldspar is present (Hower et al., 1976; Boles and Franks, 1979). Thus, presence of illite in the slope sediments suggests physical weathering of crystalline or sedimentary rocks.

5.4.1. *Composition of interstratified illite–smectite (I–S)*

Representative diffractograms from core NP90-39 are shown in Fig. 11. Determination of I–S composition and recognition of the ordering type is hampered by the presence of other clay phases, especially illite and chlorite. Using the criteria of Reynolds and Hower (1970), that I–S

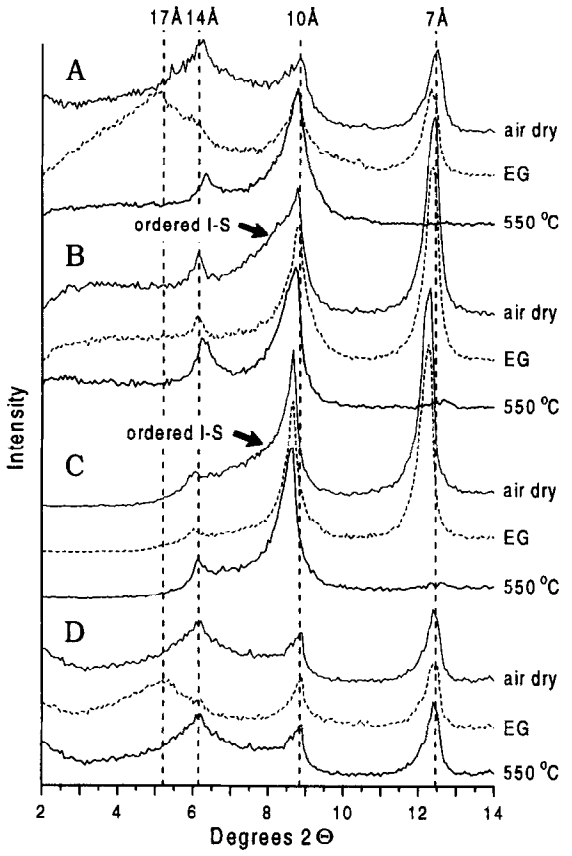

Fig. 11. Diffractograms of <2 μm fractions from core NP90-39. The samples are from (A) 87–90 cm, (B) 198–202 cm (organic-rich sediments), (C) 297–299 cm (T4), and (D) 374–278 cm. See text for details of interpretation.

with expandabilities of above 35–40% are almost always randomly interstratified and those of lower expandabilities have ordered interstratification, random ($R=0$) interlayering is identified by the presence of a 17 Å reflection after glycolation. Random interlayering is clearly present in most of the samples, but is absent from zones associated with high values of kaolinite or quartz (Fig. 10). Samples from these zones show well-defined ordering ($R=1$) with perhaps more than 60% illite layers (Fig. 11).

Studies from the North Sea (Pearson and Small, 1988; Pearson, 1990) show that I–S in burial sequences becomes more illitic with depth, and that the change from random to ordered I–S occurs at depths varying between 1400 and 3600

m. Hence, the source of the ordered I–S in the slope sediments off Svalbard might be sought in areas exposed to substantial erosion and, probably, uplift. Relatively high amounts of kaolinite and the absence of K-feldspar indicates that sedimentary rocks are a significant component of the source area. A possible source area is therefore the north-western Barents Sea which has been uplifted and eroded by approximately 3 km (Manum and Throndsen, 1978).

A similar clay mineral assemblage has been observed in samples from the Spitsbergen Bank (Bjørlykke and Elverhøi, 1975; Berg, 1991). The mineral composition of this part of the Barents Sea shows a higher content of kaolinite and mixed layered minerals than should be expected from its high-latitude position. This indicates that the clay mineral composition is controlled by glacial and subsequent marine reworking of underlying Mesozoic shales (Bjørlykke and Elverhøi, 1975).

The Spitsbergen Bank as a source area for the ordered I–S is also supported by increased concentrations of illite which may have a partial diagenetic origin, and the absence of amphibole. In addition, the palynological assemblage which is dominated by degraded material ("hot shale") and clasts of lower Jurassic and lower Triassic age show a close relationship to Jurassic and Triassic rocks in eastern Svalbard and in the Spitsbergen Bank area (Elverhøi et al., 1995a).

5.5. *Petrography of clasts (>500 μm)*

The petrographic composition of ice-rafted debris (IRD) on the slope off Svalbard can be used to make inferences about provenance, and hence, about ice flow and transportation-distances. The cores yield seven zones containing ice-rafted debris, and the six (I–VI) youngest are included in the petrographic study (Fig. 12).

IRD zones VI and V are dominated by light mudstones, with lower amounts of sandstones and quartz grains (Fig. 12A). The probable source rocks for the clastic constituents are mainly weathered rocks outside the Isfjorden and Bellsund drainage areas (see later discussion).

IRD zone IV is totally dominated by crystalline rock fragments and quartz grains (Fig. 12A). The majority of the quartz grains are most probably derived from crystalline source rocks, since there is a better coherence between these two components throughout the cores than between quartz and sandstone. The west coast of Spitsbergen, with its crystalline rocks, is a possible source area for these lithologies, but some may also originate in Fennoscandia.

The smectite-free zone (160–240 cm in core NP90-39) contains IRD in its upper part (zone III). In contrast to IRD zone IV, the ice-rafted material is totally dominated by light mudstone and sandstone fragments (Fig. 12A).

IRD zone II has been recorded in all of the slope cores, although its shape and composition varies. In general, the lower part of the zone is dominated by quartz and crystalline fragments, while the upper part is dominated by clastic rock fragments (Fig. 12A). The relatively narrow zone of crystalline rocks along the west coast of Spitsbergen is one possible source area for the crystalline components, but the sedimentary-to-crystalline ratio should have been higher if all of these fragments originated on Svalbard. In addition, the presence of chalk fragments together with the crystalline grains suggests that some of them originated in the southern part of Scandinavia, as chalk is mainly restricted to the southern part of the North Sea (Hancock, 1984; Elverhøi, 1979). Icebergs could have been transported through leads in the sea ice, similar to the present-day leads observed in the Antarctic pack ice area (Foldvik and Gammelsrød, 1988). The upcore change from crystalline to clastic lithologies through IRD zone II may thus reflect a change in source area, from Fennoscandia to the surroundings of Svalbard.

There is a closer relationship between the crystalline and clastic lithologies on the upper slope, indicating that the source area most likely was located on Svalbard. In addition, the upper slope cores contain more dark mudstones than light mudstones (Fig. 12B), of which the former are mainly of Mesozoic and Tertiary age (Elverhøi et al., 1995a). Although black shales are present on Greenland, the content of black shale fragments in the Fram Strait sediments decreases from east

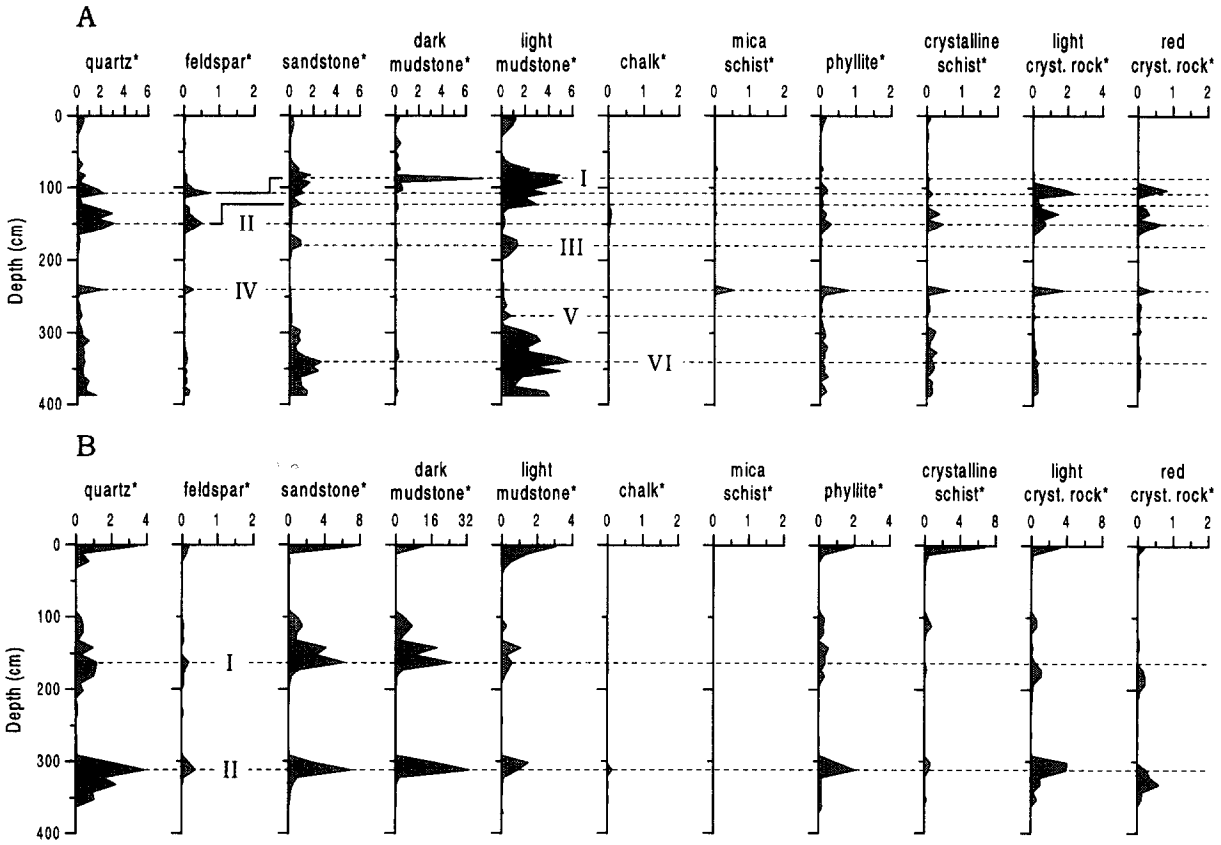

Fig. 12. Downcore variations in composition of ice-rafted debris (>0.5 mm) in cores (A) NP90-39 and (B) NP90-36B. Roman numbers refer to IRD zones. Note different horizontal scales. Nomenclature: * = number of grains (>0.5 mm)/g sediment.

to west (Spielhagen, 1991), indicating Svalbard and the Barents Sea as the main source area. Thus, a portion of the light mudstone grains that are dominating the lower slope sediments may have originated outside the drainage areas of Isfjorden and Bellsund.

The similar two-fold development has also been recorded in the youngest IRD zone (I) on the lower slope, starting with an assemblage dominated by quartz, feldspar, light-, and red crystalline rock fragments (Fig. 12A). The only difference is that the upper part of the zone also is associated with dark mudstones, indicating a closer relationship between the lower slope sites and Svalbard at that time. This is supported by the relatively high content of red crystalline rock fragments, typical for the northern and central parts of Svalbard (Sørflaten, 1993).

6. Lithofacies

The lithofacies described are sorted into five groups based on their sedimentary characteristics: (1) laminated-to-layered mud, (2) massive mud, (3) graded silt, sand and gravel, (4) homogenous diamicton, and (5) heterogeneous diamicton. Each facies association is attributed to a different depositional environment (Tables 4, and 5). These facies are generally laterally continuous between different cores (Fig. 13), and they occur in more than one stratigraphic position.

6.1. Laminated-to-layered mud

Laminated-to-layered mud (Fl) is common in all cores, particularly on the upper slope (Fig. 13A,B). These deposits are confined to the

Table 4
Lithofacies codes and sedimentary characteristics

Code	Lithofacies type	Sedimentary structures	Interpretation
F	*Fine-grained (mud)*		
Fm	massive mud	massive, bioturbated, clast-poor	hemipelagic deposit
Fl	laminated to layered mud	alternating clay, silt, and fine sand laminae	turbidite flow- or contourite deposit
D	*Diamict*		
Dm	matrix supported	homogenous, matrix-supported; very poorly sorted clay/silt/sand/gravel admixture	debris flow deposit (fan) or mixture of hemipelagic and ice-rafted debris (lower slope)
Ds	stratified	matrix-supported; slight stratification	hemipelagic-, ice-rafted-, and bottom current deposit
Dg	graded	matrix-supported; clast content generally normally graded	debris flow deposit or hemipelagic deposit w/ waning clast content
S	*Sand and silt*		
Sg	graded	grading; no bedding	low-concentration turbidite flow deposit
Sm	massive	no grading/bedding	Turbidite flow deposit
G	*Gravel*		
Gg	graded	graded; no bedding	high-concentration turbidite flow deposit
–d	dropstones		
–b	bioturbated		
–(l)	slightly laminated		
–(s)	sandy		
–(r)	reworked	clast-supported	lag deposit
–(d)	disturbed		

Table 5
Colour codes

Code	Colour	Code	Colour
g	grey	lob	light olive brown
dg	dark grey	ob	olive brown
vdg	very dark grey	dgb	dark greyish brown
og	olive grey	vdgb	very dark greyish brown
dog	dark olive grey	rb	reddish brown
o	olive		

organic-rich zones that succeed each high-production zone (Fig. 6A,B). The lamination is fairly indistinct and consists of alternating thin, silt-rich and silt-depleted lamina. Individual laminae are generally poorly defined. Typical colours are grey, dark grey, very dark grey, black, strong brown, dark yellowish brown, olive grey, and dark olive grey. Where black and grey coloured mud occur together, the former is often found below the latter (Fig. 13C).

The layered mud consists of 4–5 cm thick zones of clay-rich mud and sand/silt-rich mud. Coarse grains are generally sparsely scattered. Bioturbation seems to be suppressed on the lower slope, but is more common on the upper slope (Fig. 13A). The two facies types seem to alternate, indicating a cyclic depositional pattern. Basal and upper contacts are sharp, indicating a rapid change in sedimentary processes. Thin sand layers and sand lenses are often associated with laminated mud, especially on the lower slope. Deformation and erosion structures occur within this facies (Fig. 13C), and the former is most likely an effect of sampling.

There are several independent lines of evidence to suggest that the laminated-to-layered sediments were deposited by a combination of downslope and semi-permanent bottom (contour) currents. Firstly, the downslope component is reflected by the regional distribution of this lithofacies, which shows a general decrease in thickness from the

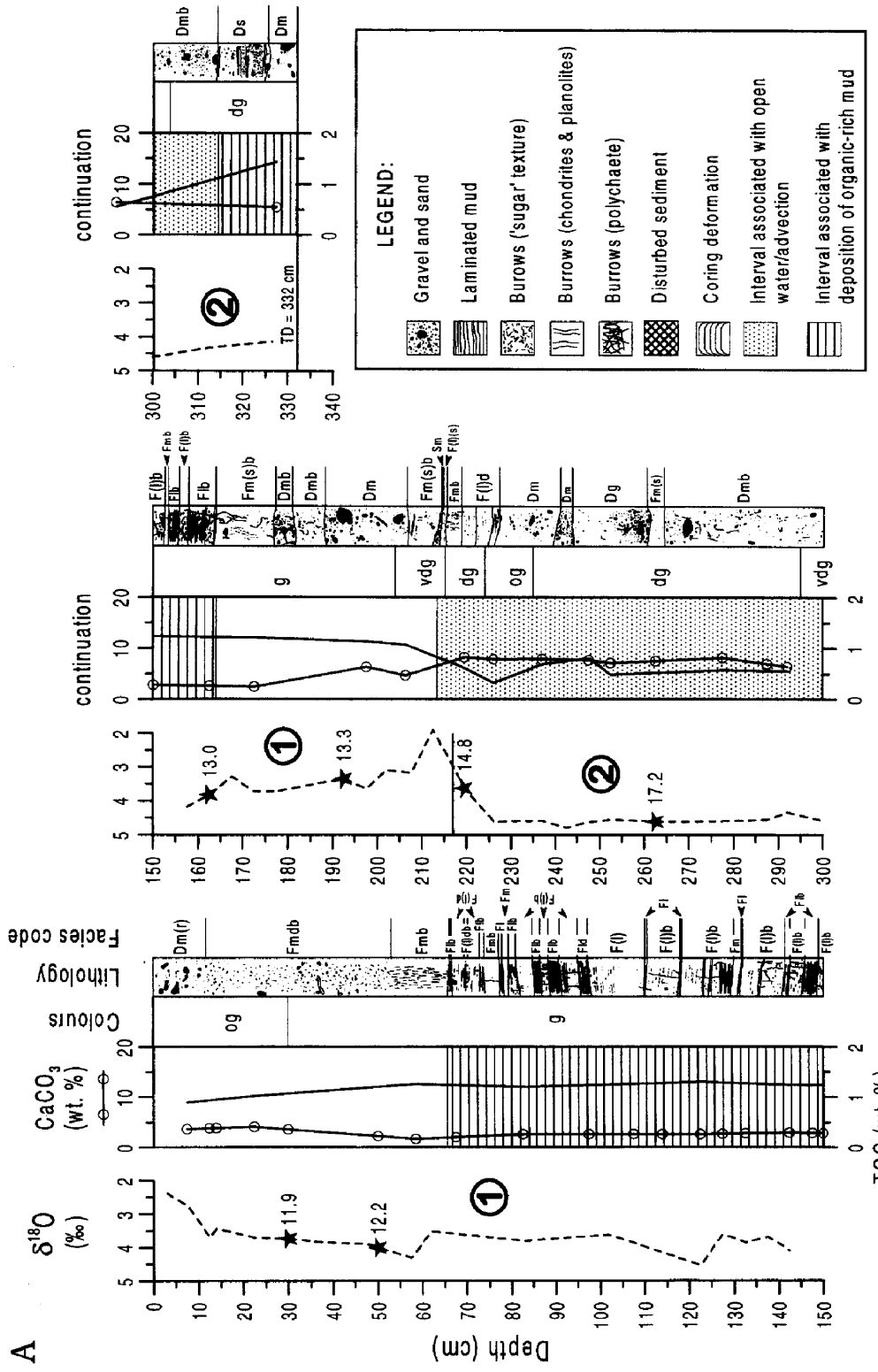
A
δ18O (‰)
CaCO3 (wt. %)
Colours
Lithology
Facies code
Depth (cm)
TOC (wt. %)
continuation
TD = 332 cm
LEGEND:
Gravel and sand
Laminated mud
Burows ('sugar' texture)
Burrows (chondrites & planolites)
Burrows (polychaete)
Disturbed sediment
Coring deformation
Interval associated with open water/advection
Interval associated with deposition of organic-rich mud

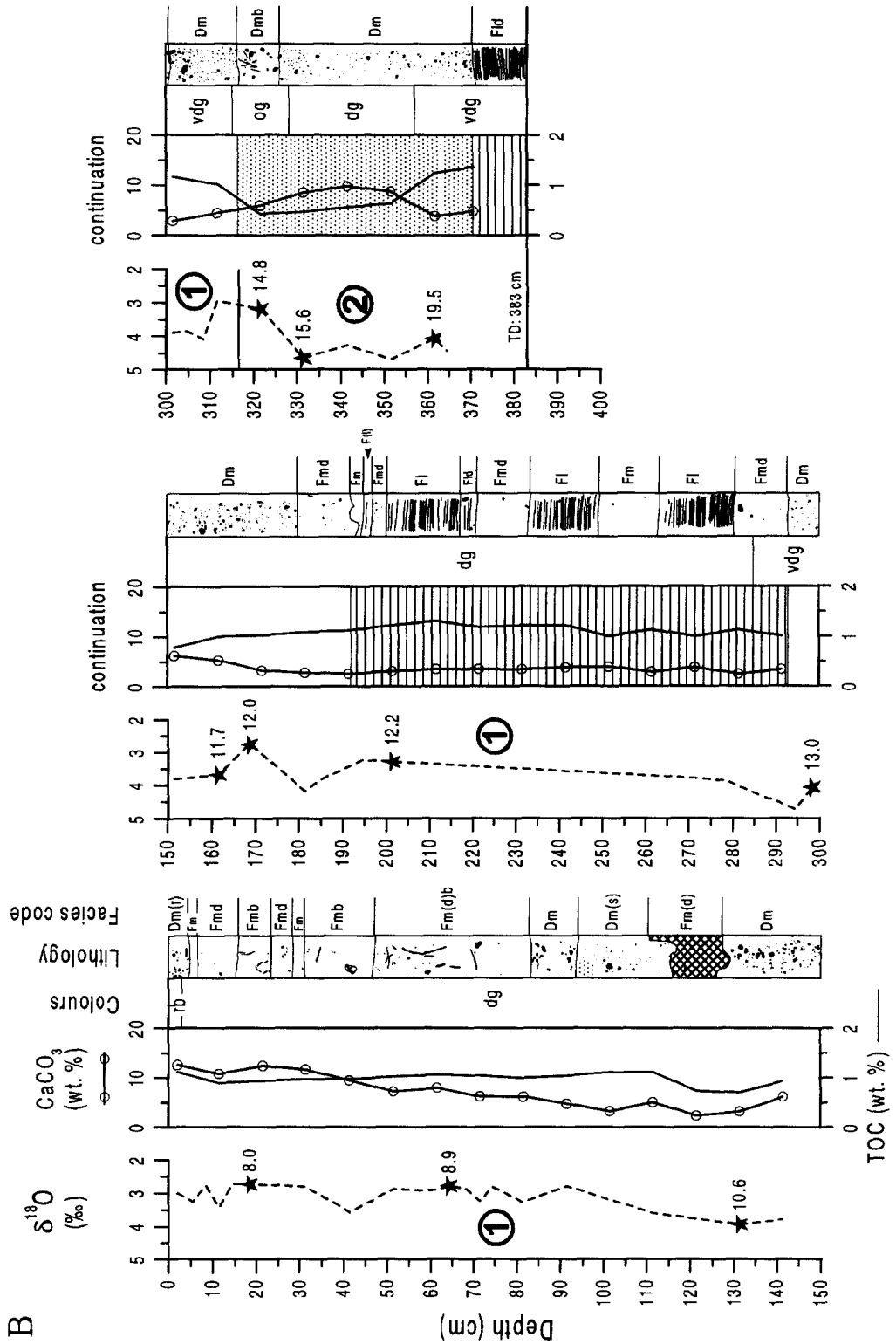
B
Depth (cm)
δ18O (‰)
CaCO3 (wt. %)
TOC (wt. %)
Colours
Lithology
Facies code
continuation
TD: 383 cm
14.8
15.6
19.5
11.7
12.0
12.2
13.0
8.0
8.9
10.6

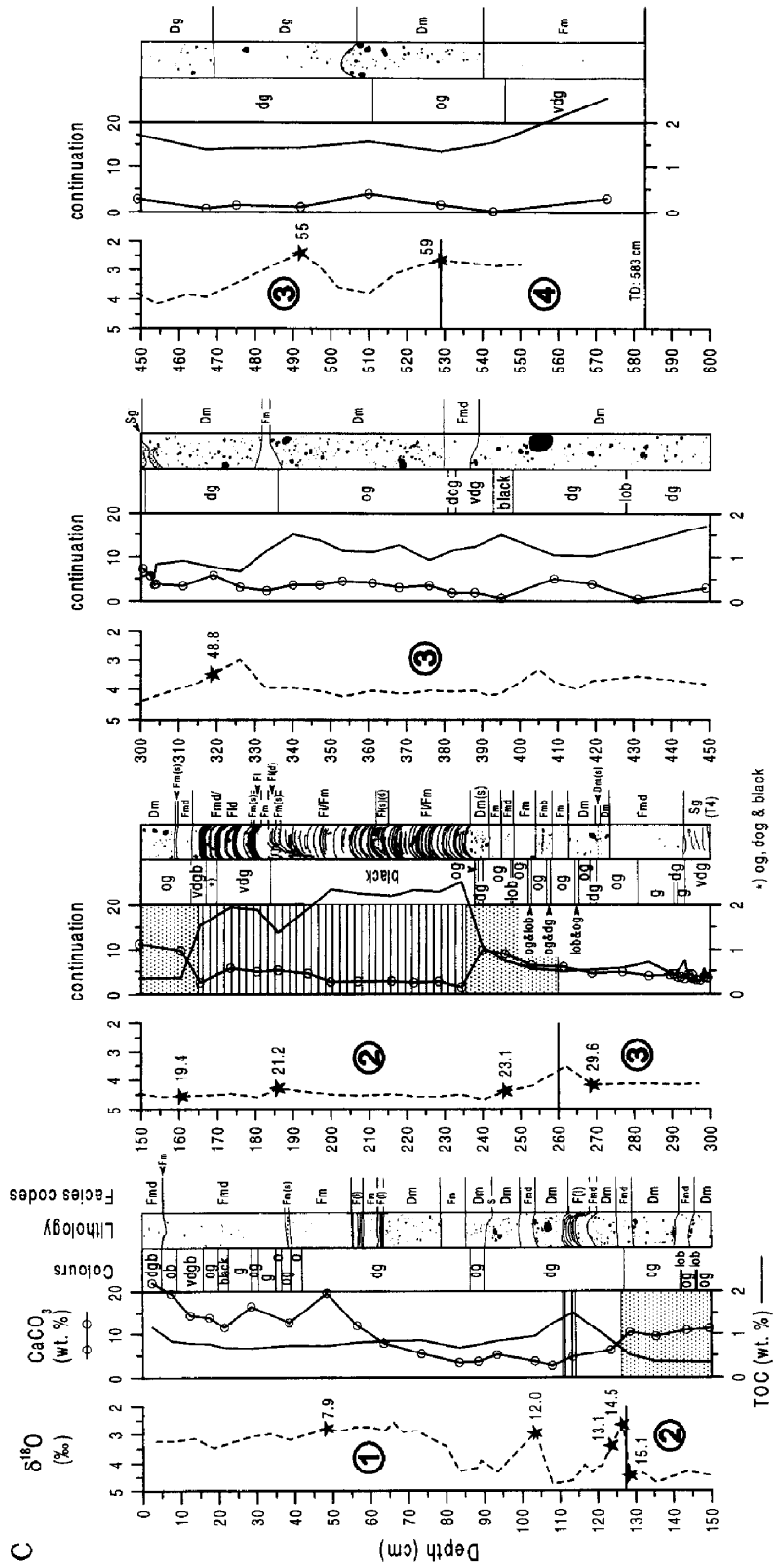
Depth (cm)
δ18O (‰)
CaCO3 (wt. %)
Colours
Lithology
Facies codes
TOC (wt. %)
continuation
TD: 583 cm
*) og, dog & black

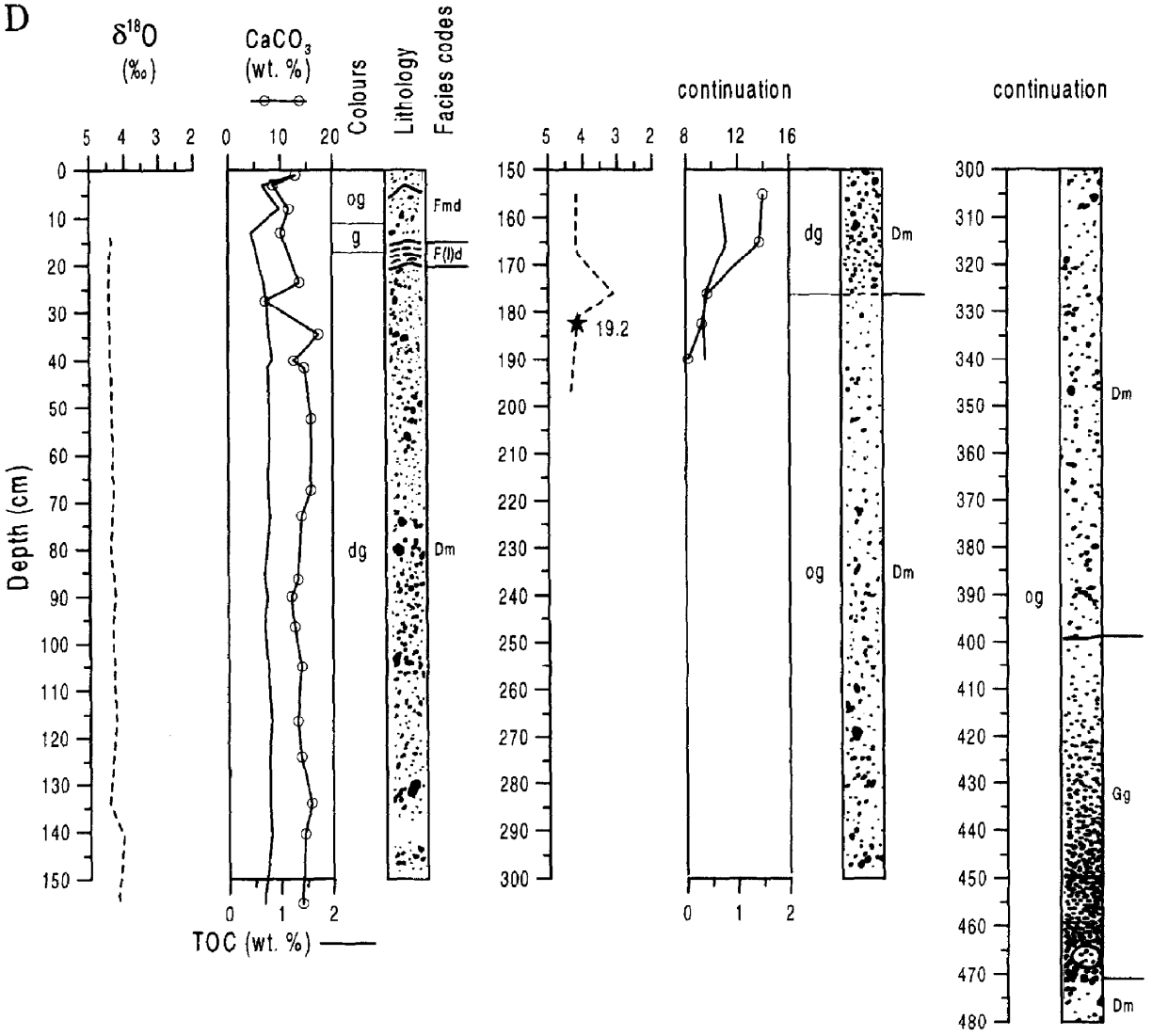

Fig. 13. Composite diagrams showing oxygen isotope records, TOC- and $CaCO_3$ records, colours, and lithofacies from core (A) NP90-12B, (B) NP90-36B, (C) NP90-39 and (D) NP90-18C. Filled stars and corresponding numbers represent ^{14}C ages and age estimate based on correlation of oxygen isotope records (Dokken, 1995). Numbers inside circles refer to Isotope Stages, and ages for isotope-stage boundaries are from Henrich and Baumann (1994). Lithofacies codes and sedimentary characteristics are shown in Table 4, and colour codes are shown in Table 5. The heterogeneous diamictons (Dm) between 300 and 540 cm in core NP90-39 represent four Middle Weichselian ice advances, and the oldest is correlated with the Glaciation E recorded at Kapp Ekholm in Isfjorden. The diamicton at 263–274 cm reflects most likely an ice advance in Fennoscandia. Note that core NP90-39 shows signs of coring deformation along sides.

upper slope (Fig. 13A,B) towards the deep sea (Fig. 13C). Secondly, relatively high (up to 141 cm/ka) linear sedimentation rates (Fig. 14) suggest at least episodic turbidite sedimentation, since sedimentation rates associated with fine-grained contourites usually are less than 2–15 cm/ka (see reviews by Stow and Holbrook, 1984; Stow, 1985). The existence of trace fossils within these deposits (Fig. 13A) also suggest episodic sedimentation and development of burrows during periods of continuous (hemipelagic) and semi-continuous (contour) accumulation when

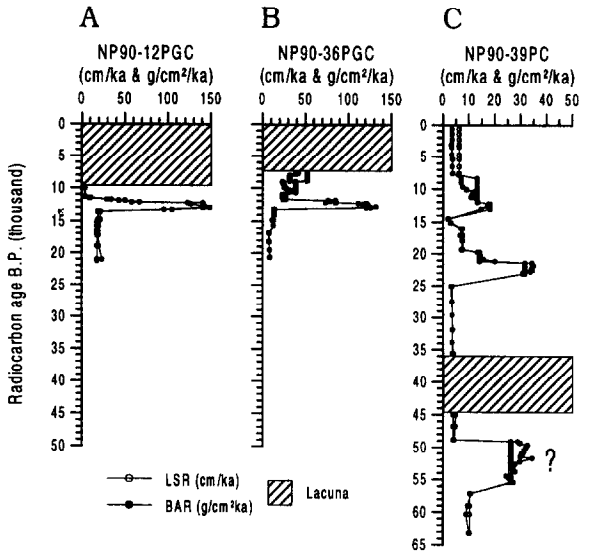

Fig. 14. Linear sedimentation rates (LSR) and bulk accumulation rates (BAR) in cores (A) NP90-12B, (B) NP90-36B and (C) NP90-39. Values before 48.8 ka are only proxy, since AMS dates are lacking in the lower part of core NP90-39.

sedimentation rates were lower. This relationship clearly shows that using constant sedimentation rates between fix-points as a proxy is not a precise approach. Finally, the clear relationship between these deposits and the Spitsbergen Bank, as indicated by the mineralogical and palynological studies, suggest a combination of fast-flowing downslope currents and more slowly moving contour currents.

6.2. *Massive mud*

The massive mud (Fm) is up to 1 m thick and is related both to laminated-to-layered mud and clast-rich diamictons. As an example, core NP90-36B shows a nice alternating pattern of laminated and massive mud between approximately 200 and 295 cm (Fig. 13B), indicating a cyclic change in the depositional processes. The massive mud contains occasional lonestones, and in places this facies becomes more like a diamicton (Fmd), containing sparse pebbles, larger clasts and some sand (Fm(s)).

Signs of bioturbation are rare, but where burrows are identified, they show up as a small-scaled "sugar" texture, *polychaete* tubes (Trypanites ichnofacies; Frey and Pemberton, 1984), mm-sized *Chondrites*, and cm-sized *Planolites* (Cruziana ichnofacies).

The sediments show a large variety of colours, including olive grey, grey to very dark grey, black, strong brown, dark brown, light olive brown, olive brown, greyish brown to very dark greyish brown, and dark yellowish brown.

This facies is interpreted as hemipelagites deposited by slow settling through the water column in the absence of any substantial bottom current activity. Hemipelagic muds have no primary sedimentary structures and contacts between beds are always gradational (Stow, 1985). Variable amounts of IRD and bioturbation are indicative of slow and persistent deposition from ice-rafting and hemipelagic settling (Stow and Holbrook, 1984; Gonthier et al., 1984). The existence of burrows indicates low sedimentation rates and oxygenated bottom waters. Thus, intensively bioturbated zones indicates episodes of increased oxygen supply, probably supplied by bottom currents (Stow, 1979; Chough and Hesse, 1985) or during periods of increased vertical ventilation.

6.3. *Graded silt, sand and gravel*

This facies consists of graded silt and sand (Sg), and locally graded gravel (Gg). It is commonly less than 15 cm thick and more or less confined to the lower slope. The beds contain predominantly silt to fine sand and are marked by erosional contacts (Fig. 13). The sand-silt layers are generally laterally continuous between core sites, and layer T4 especially seems to cover a fairly large area, since it is present in cores NP90-38C, -39 and -40B (Fig. 4B). The silt and sand layers grade into laminated or massive mud.

A relatively thick (~70 cm) graded gravel bed (Gg) was recognised below a debris flow deposit on the upper part of Isfjorden Fan (Fig. 13D). The bed consists of pebbles at the base and fines upwards to medium sand in the top (Fig. 4C). The lower boundary is sharp, clearly erosional, and deformed. Intercalation of clay-rich bodies, obviously derived from the clast-depleted sediments below, occurs in the lower part of the bed.

This facies is interpreted to be deposited from turbidity currents, because they all show a sequence of structures and grain-size through single-event deposits from a few centimetres to a few tens of centimetres in thickness. These are closely analogous to the classical Bouma sequence for fine- and coarse-grained turbidites (Bouma, 1962), but they only form fining-upward sequences that are composed of a basal silt-, sand- or pebble unit and an overlying homogenous or laminated mud representing the topmost part of a turbidite sequence (Stow and Piper, 1984). Thus, only partial Bouma sequences have been developed.

Our provenance studies suggest that the turbidite T4 contains clay particles from the Spitsbergen Bank area. We therefore propose that it was generated on the northern flank of Storfjorden Fan which is located between Spitsbergen and Bjørnøya (Fig. 1). The texture of the coarse-grained turbidite located on the Isfjorden Fan clearly reflects the source material, which most likely consists of unsorted glacial sediments originally deposited close to the shelf edge. These sediments are not attached to feeder channels, but are suspected to be incorporated into initial downslope movement via debris flows, which, according to Wright and Anderson (1982), may produce turbidity currents as they move downslope.

6.4. *Homogenous diamicton*

Homogenous diamicton (Dm) occurs in lithologically distinct beds up to 6–7 m thick. Pebble- to very coarse sand-sized clasts are randomly dispersed in a mud matrix of diverse colours (grey to very dark grey, olive, olive grey, black, dark greyish brown, dark yellowish brown, strong brown, dark brown, and weak red). Both size and distribution of clasts vary between the individual beds, and in places this facies becomes more like a massive mud, containing sparse pebbles. Trace fossils are not common in this facies and are mostly restricted to the interfan areas on the upper slope (Fig. 13A).

Core NP90-18C penetrates the flanks of two lens-shaped sediment bodies on the upper part of Isfjorden Fan (Fig. 15) which we interpret as debris flow deposits. The corresponding section in

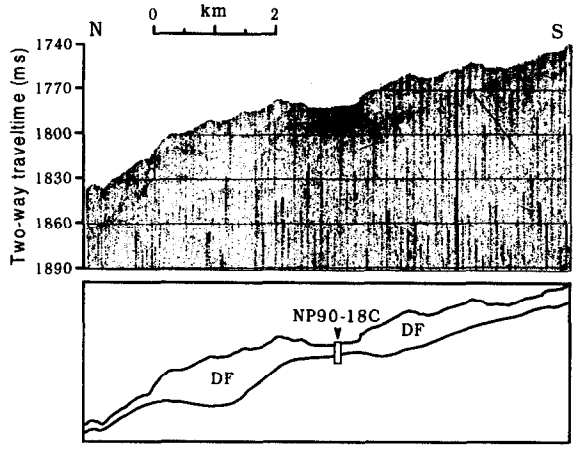

Fig. 15. Part of deep tow Huntec Boomer line NP90-121 (above) and interpreted line drawing (below), showing debris flow deposits (*DF*) on the Isfjorden Fan. Core NP90-18C penetrates the section between two debris flow deposits. For location, see Fig. 1.

the core is located between 20 and 175 cm (Fig. 13D). A debris flow origin is in agreement with findings of a shallow-marine fauna assemblage (T. Slinning, unpublished data). Based on textural and structural characteristics, we suggest that the homogenous diamictons below 175 cm in core NP90-18C also represent debris flow deposits. This sedimentary facies forms therefore approximately 85% of the core. This conclusion is in accordance with the uniform character of the physical properties of the upper fan sediments (water content and wet bulk density; Fig. 3). In addition, a sedimentological study of the southern flank of the Bjørnøya Fan (Yoon et al., 1991) which suggests that thick-bedded (>1 m), disorganised mud with coarse-grained clasts dispersed in fine matrix are considered as debris flow deposits, and the seismic characteristics of the Isfjorden Fan (Andersen et al., 1994) which indicates that it consists of numerous sediment bodies of considerable length, giving a hummocky appearance on strike lines (Fig. 16). It is also in agreement with studies of the Storfjorden and Bjørnøya fans (Laberg, 1994), suggesting that sediments deposited near the shelf edge were subsequently moved downslope, mainly as large debris flows. Thus, debris flow deposits form the majority of sub-

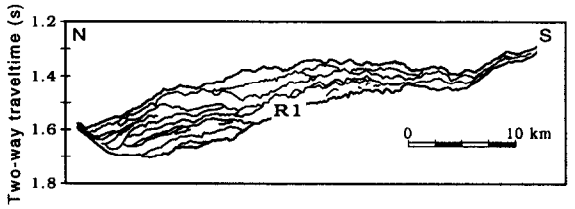

Fig. 16. Line drawing of part of sleeve gun line NP90-303, showing slumped sediment bodies on the upper part of Isfjorden Fan. Reflector *R*1 represents the lower boundary of the youngest sequence defined on the western Svalbard slope (Andersen et al., 1994), tentatively dated to 200 ka (Elverhøi et al., 1995b) or younger than 440 yr (Sættem et al., 1992). For location, see Fig. 1.

marine fans on glaciated high northern latitude margins.

We can not rule out the possibility that the homogenous muds deposited on the lower slope and on the upper slope between the submarine fans were transported by debris flows. An argument in favour of this is the apparent inconsistency in some of the sedimentological records. For example the relationship between organic carbon and carbonate as described by Henrich et al. (1989) disappears below T4 (Fig. 6B). However, we suggest that hemipelagic sedimentation with major releases from sediment-rafting dominates these areas. Firstly, the smooth topography of the interfan and lower slope areas as inferred from wide-angle side scan sonar recordings (Vogt et al., 1990; Crane and Solheim, 1995) does not indicate the existence of debris flows. Secondly, burrows are present (Fig. 13A), reflecting slow and persistent emplacement, and no deformation structures as a result of traction are present. Finally, because biostratigraphic correlation along the western Svalbard–Barents Sea margin (Dokken, 1995), indicates hemipelagic sedimentation.

6.5. Heterogeneous diamicton

The heterogeneous diamicton consists of three sub-facies, a graded diamicton (Dg), a sandy, slightly stratified diamicton (Ds), and a reworked diamicton (Dm(r)). The graded diamicton is most common on the lower slope and is characterised by a pebble-rich lower and a pebble-depleted upper part. The upper boundary is diffuse; the lower boundary is well defined, but no erosional or deformation structures have been observed. Colours vary from greyish to brownish (grey to very dark grey, olive, olive grey, olive yellow, and dark yellowish brown). The graded diamicton is interpreted as having been deposited by a combination of hemipelagic sedimentation and ice-rafting. The lower part of these deposits may therefore reflect a period during which release of large quantities of icebergs gave a distinct IRD signal. A gradual reduction in ice-rafting with time and/or increased hemipelagic sedimentation caused reduction in the relative amount of dropstones.

The stratified diamicton has only been observed in a single bed in the lower part of core NP90-12B (Fig. 13A), and represents the upper part of the corresponding laminated-to-layered zone in core NP90-36B (Fig. 13B). It consists of a dark grey diamicton complex containing many stringers of silt. Both the upper and lower contacts are well defined.

The uppermost 5–10 cm of cores NP90-12B and -36B consist of an olive grey and a rusty brown mud, respectively, with a high content of clasts (Dm(r)). Since the diamictons are restricted to the core tops (Fig. 13A), we suggest that they represent lag deposits. This is in agreement with the physical properties (e.g., water content) and the stratigraphical records (AMS and oxygen isotope), which indicate that the youngest part of cores NP90-12B and -36B has been eroded.

7. Depositional facies and glacial conditions

Stratigraphic relationships among the facies on the western Svalbard slope indicate a recurring pattern that allows delineation of several phases during the final build-up and the subsequent recession of the Svalbard–Barents Sea Ice Sheet.

7.1. Isotope stage 3

Several studies have reported a major increase in ice-rafted and terrigenous debris during glacial periods in the North Atlantic region (Ruddiman and McIntyre, 1976; Fillon et al., 1981; Alam et al., 1983; Heinrich, 1988, 1989). This is also the

case during Isotope Stage 3 along the western Svalbard margin. At that time (59–27 ka), hemipelagic mud with ice-rafted material, hemipelagic mud, and turbidites prevailed (Fig. 13C). Thus, the Middle Weichselian was characterised by several periods of extensive iceberg production and ice-rafting in the north-eastern part of the Norwegian–Greenland Sea. The abundance of light mudstone and sandstone clasts suggests that the main source was located in the eastern Svalbard–Barents Sea area, and not in Fennoscandia or western Svalbard. The lack of iceberg-production in the two latter areas is in agreement with the general absence of amphibole below T4 (Fig. 10), suggesting that before ~44 ka, the material was not coming from areas with crystalline bedrock. The assumption of small ice caps in Fennoscandia and the inner fjord areas of Svalbard is in accordance with terrestrial data suggesting that the ice sheets of Fennoscandia (Mangerud, 1991) and Svalbard (Landvik et al., 1992; Mangerud and Svendsen, 1992) were limited in size or probably did not exist during most of Isotope Stage 3.

The ice-rafted debris around 59–55 ka (Fig. 17) can be correlated with the Middle Weichselian Glaciation E (Mangerud and Svendsen, 1992) recorded at the Kapp Ekholm section in Isfjorden (Fig. 1). The subsequent deglaciation coincides with the upper end of the IRD peak (Fig. 17) and a light $\delta^{18}O$ peak at 55 ka (Fig. 13C). The pronounced IRD peaks between 54 and 27 ka demonstrate that there may have been more glaciations than recorded on Svalbard, and the distribution of heterogeneous diamictons in core NP90-39, although the record is discontinuous due to erosion, suggests that there were four glacial advances (Fig. 13C). This is partly supported by amino acid measurements at Kapp Ekholm, which indicates that glaciations may have occurred in the inner fjord areas of Svalbard until 40 ka (Mangerud and Svendsen, 1992). The presence of a Barents Sea Ice Sheet may explain why the global eustatic sea level during the penultimate interstadial (following Glaciation E) was lower than today (Mangerud and Svendsen, 1992).

Although it appears that the ice-rafted material at 30 ka (Fig. 17) reflects an ice advance in the

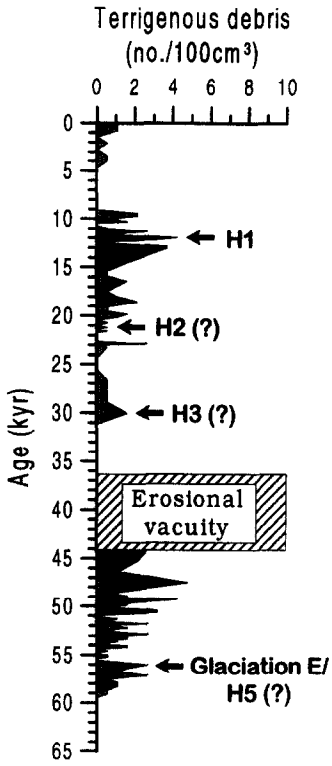

Fig. 17. Numbers of terrigenous grains (>2 mm/100 cm³) in core NP90-39 plotted against ^{14}C age. *H1*, *H2*, *H3*, and *H5* represent episodes when Heinrich layers were deposited.

Barents Sea area, findings of shell fragments in glacially reworked sediments dated between 22 ka and approximately 40 ka (Elverhøi et al., 1993), suggest that the Barents Sea was ice-free during this period. The IRD peak is therefore assumed to reflect a glacial advance recorded in the northern North Sea (Sejrup et al., 1994) and northern Norway (Vorren et al., 1988; Alm, 1993) around 30 ka.

In conclusion, we suggest that the Middle Weichselian ice sheet remained in the eastern Svalbard–Barents Sea area at least until ~44 ka. In addition, it seems that ice sheets at high northern latitudes fluctuated more frequently than previously thought.

7.2. *Late Weichselian ice growth*

According to our data from the western Svalbard slope, the occurrence of a zone character-

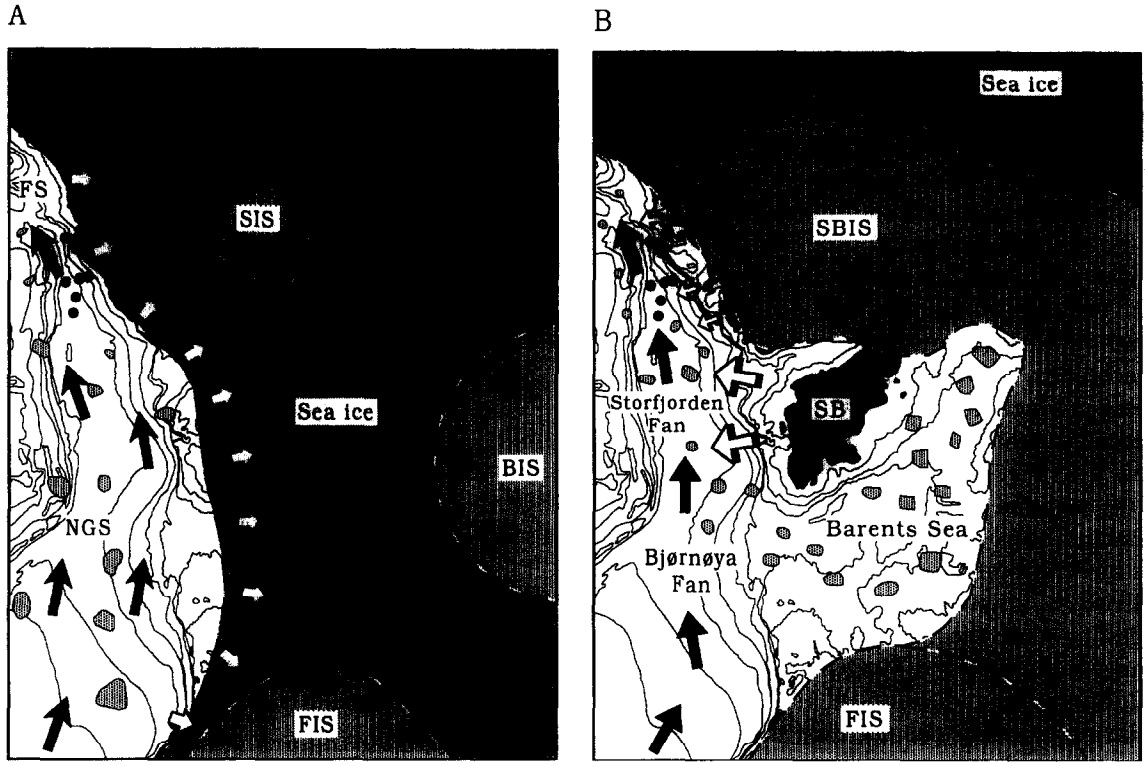

Fig. 18. Schematic maps showing (A) advection of warm Atlantic water (large, filled arrows) into the Norwegian–Greenland Sea providing moisture (open arrows) for the nucleating Svalbard–Barents Sea and Fennoscandian ice sheets, and (B) erosion of the shelf banks during ice-growth due to eustatic sea-level lowering. *NGS*= Norwegian–Greenland Sea; *SIS*= Svalbard Ice Sheet; *BIS*= Barents Sea Ice Sheet; *FIS*= Fennoscandian Ice Sheet; *SBIS*= Svalbard–Barents Sea Ice Sheet; *SB*= Spitsbergen Bank; filled circles= core sites.

ised by high foraminiferal concentrations (Hebbeln et al., 1994; Dokken, 1995) and polychaete burrows (Fig. 13C), suggest that relatively warm water from the North Atlantic Ocean was advected into the Norwegian–Greenland Sea between 27 and 22.5 ka (Fig. 18A). Thus, the onset of full glacial conditions was associated with relatively warm surface waters close to the continental margin of Svalbard, favouring increased organic production, generally low iceberg production (Fig. 17), low (<3.5 g cm^{-2} ka^{-1}) bulk accumulation rates (Fig. 14), and well-oxygenated bottom waters. It is very likely that the seasonally ice-free waters were an important moisture source during the nucleation of the Late Weichselian Svalbard–Barents Sea Ice Sheet (Hebbeln et al., 1994) that occurred during this period (Mangerud and Svendsen, 1992). The IRD zone (IV) appearing at the end of this period, probably reflects calving of the Fennoscandian Ice Sheet, since it is totally dominated by crystalline clasts. Thus, it appears to reflect the glacial retreat recorded close to Andøya in northern Norway (Vorren et al., 1988) and the North Sea (Sejrup et al., 1994) around 23 ka.

At approximately 22.5 ka, the IRD production terminated and instead a substantial increase in hemipelagic sedimentation and frequency of turbidity currents occurred (Fig. 13C). Similar sediments have also been described from full glacial stages in central Baffin Bay by Aksu and Piper (1987). They suggest that the lack of IRD deposition may be related to reduced calving, lower sediment concentration in the icebergs, or an absence of iceberg melt. However, though these processes explain the paucity of ice-rafting during

the part of glacials characterised by heavy isotopes, they do not explain the rapid accumulation of dark, fine-grained organic-rich sediments that has accumulated in the Norwegian–Greenland Sea (Henrich et al., 1989).

Hebbeln et al. (1994) relate the fine-grained organic-rich deposits to a minor stand-still during the final growth of the Svalbard–Barents Sea Ice Sheet. Rather, we suggest that deposition of these sediments was indirectly controlled by the final growth of the Svalbard–Barents Sea Ice Sheet. As apparent from glaciation curves (Mangerud and Svendsen, 1992; Elverhøi et al., 1993) the ice started to grow sometime between 30 and 20 ka. Consequently, the global eustatic sea level was lowered by at least 100 m (Fig. 18B), exposing the shallowest part of the Spitsbergen Bank to alluvial and shallow-marine processes. As a result, large quantities of dark, fine-grained organic-rich sediments were moved from the shelf to the Norwegian–Greenland Sea. This is in agreement with Yoon et al. (1991), whose textural and structural description of slope sediments, suggest that closely spaced, thin (< 1 mm) laminae, an absence of bioturbation, and a darker sediment colour are suggestive of downslope bottom currents with a high sediment fallout rate. It is also supported by the presence of turbidites on the lower slope (e.g., T3), since the abundance of turbidites in the oceans during glacial periods is generally accounted for by sea-level lowering (Shanmugam and Moiola, 1982).

Deposition of fine-grained sediments continued until 19.5 ka (Fig. 13C). The last 1500 years of this period were associated with iceberg production and deposition of light mudstones (IRD zone III) on the lower slope (Fig. 12A). Since the clasts were deposited together with the organic-rich sediments, and the upper slope sediments are dominated by dark mudstones (Fig. 12B), we suggest that most of the icebergs passing over the lower slope sites at that time were generated in the Barents Sea area.

7.3. Peak glaciation

The depositional environment changed dramatically around 19.5 ka, by which erosion of the bank areas ceased and, according to Hebbeln et al. (1994), warm Atlantic water and icebergs from the North Sea entered the Norwegian–Greenland Sea once again. They also suggest that the Svalbard Ice Sheet expanded to the shelf edge during this second Atlantic water advection event (19.5–14.5 ka) and that the marine-based part of it started to disintegrate shortly after reaching its maximum position. However, the findings of debris flow deposits of glacial maximum age suggest that the ice front was located close to the shelf edge no later than approximately 19 ka rather than around 15 ka. An ice sheet covering most of the shelf would explain why input of fine-grained shelf sediments stopped around 19.5 ka, since an ice sheet would protect the shelf banks against alluvial and marine processes.

We therefore suggest a faster marginal advance (Fig. 19), similar to the rapidly moving Laurentide Ice Sheet lobes during the Late Weichselian glaciation (Clayton et al., 1985, 1989). A glacier front may prograde rapidly and produce a gentle ice-surface profile if the yield stress at the base of the glacier is less than the normal yield stress within the glacier (Clayton et al., 1985), which is often about 100 kPa (Paterson, 1994). In other words, if the ice rests on a continuous layer of clay-rich sediments, such as those on the western Svalbard shelf, the subglacial pore pressure may become great enough to support much of the glacier's

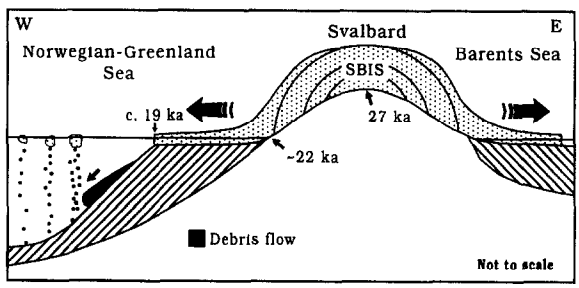

Fig. 19. Conceptual model for the Late Weichselian ice-sheet growth on Svalbard. Advection of Atlantic water to the NGS is assumed to have been an important moisture source for the ice-nucleation at 27 ka. Glacial growth was accelerated around 22.5 ka, when the ice margin reached the shelf off Svalbard, producing a relatively thin ice with a gentle surface slope. *BS*= Barents Sea; *SBIS*= Svalbard–Barents Sea Ice Sheet.

weight, and as a result, make the ice move rapidly by bed deformation or sliding.

The second seasonal open-water event was therefore not necessarily fully responsible for the final build-up of the Svalbard–Barents Sea Ice Sheet as suggested by Hebbeln et al. (1994). Our two-step model which includes a relatively slow build-up between 27 and approximately 22.5 ka followed by a rapid advance forming a relatively thin ice, may fit better with mass-balance calculations by Siegert and Dowdeswell (1995) of the last ice-sheet growth in the Barents Sea area, because, according to their model, the formation of a thick ice cap covering most of Svalbard and the Barents Sea within a time frame of approximately 7000–8000 yr is problematic.

The radiocarbon ages suggest that accumulation rates of hemipelagic sediments were reduced on the slope as the ice expanded onto the shelf (Fig. 14), and stayed low until approximately 13.5 ka. As opposed to the general trend, accumulation rates on the submarine fans were most likely greatest during peak glaciation (Elverhøi et al., 1995a). This is supported by the dates obtained from the base of the debris flow deposits recognised on the upper slope, and heavy (4–4.5‰) glacial $\delta^{18}O$ values throughout the sediments (Fig. 13D), reflecting that the debris flows were released some time during glacial maximum. We therefore conclude that sedimentation is focused onto the submarine fans during peak glaciation and more dispersed during periods with less ice sheet cover.

7.4. Break-up of the marine-based Svalbard-Barents sea ice sheet

The initial break-up of the ice sheets covering the Svalbard and Barents Sea area is recorded as a light $\delta^{18}O$ peak in the slope sediments, occurring at approximately 14.5 ka (Fig. 13), interpreted as a meltwater signal. Radiocarbon dates along an east–west profile following the Isfjorden Trough indicate that the ice front retreated rapidly (Elverhøi et al., 1995a). This is in agreement with the relatively low bulk accumulation rates on the slope between 15 and 14 ka (Fig. 14). Andersen et al. (1995) suggest that the low accumulation rates immediately following the break-up of the marine-based Fennoscandian Ice Sheet reflect a rapid retreat of a thin ice sheet. Based on this idea, together with our growth model, we suggest that the ice sheet that covered the shelf off Svalbard was relatively thin during the glacial maximum and therefore underwent a rapid retreat caused by the small rise in sea level close to 15 ka (Fairbanks, 1989). Although there are too many uncertainties to allow us to estimate the size of this ice sheet from the amplitude of the isotopic light event recorded, the size of a comparable meltwater peak recorded in the Fram Strait has been suggested to be equivalent to $\sim$15 m of eustatic sea-level rise (Jones and Keigwin, 1988).

Bulk accumulation rates were low during the first phase of retreat and there was a dominance of hemipelagic sedimentation and ice-rafting to the slope, implying that melting of icebergs was more important than direct supply of fine-grained sediments at the ice front. The close relationship between the clastic and crystalline components on the upper slope suggest that most of the coarse, unsorted debris was generated in the Svalbard area. The record of the lower slope cores is slightly more complicated, since the crystalline peak leads the clastic peak (Fig. 12A). A possible explanation is that the lower slope sites detect the onset of the disintegration of the Fennoscandian Ice Sheet prior to that of the Svalbard Ice Sheet.

An extensive ice recession close to 14.5 ka is required in order to produce the distinct light isotope peak recorded in the lower slope cores (Fig. 13C). But, since the ice did not leave the western Svalbard shelf until 12.5 ka (Mangerud et al., 1992; Elverhøi et al., 1995a), this meltwater pulse appears to indicate the onset of decay of the major Barents Sea Ice Sheet, as suggested by Elverhøi et al. (1993) and Polyak et al. (1995). Similar meltwater signals have been recorded in the Arctic Ocean (Stein et al., 1994b) and on the East Greenland continental margin (Nam et al., 1995). Thus, the almost parallel trends of the oxygen isotope records may be indicative of contemporaneous variations of the Barents Sea and Greenland ice sheets, or they may signal, as proposed by Stein et al. (1994b), an increased export of low-saline waters from the Arctic to the East Greenland Current controlled by the supply of

meltwater from Siberian rivers and the decay of the Barents Sea Ice Sheet.

Shell dates from tills on the shelf indicate a glacial re-advance that ended shortly after 12.4 ka (J.I. Svendsen, unpublished data). The proposed ice advance coincides with the thick sequence of stratified and massive muds on the upper slope (Fig. 13A,B). We therefore suggest that these sediments were accumulating during a period (~13–12 ka) during which the ice margin was located on the inner shelf and the sea level was low enough to allow reworking of the bank deposits on the western Svalbard shelf. Although the dates suggest generally high accumulation rates (Fig. 14), burrows and zones containing massive mud suggest a quickly changing environment, probably due to a rapidly fluctuating sea level.

The short-lived ice advance ended close to 12 ka, and the following ice retreat was similar to the initial break-up around 14.5 ka, as the ice margin disintegrated principally by iceberg calving leading to unsorted coarse sediments deposited on the entire slope. Since the youngest IRD zone (I) recorded on the lower slope shows a similar development as its predecessor (zone II) we suggest that an area containing crystalline fragments (e.g., Fennsocandia) delivered coarse grains to the lower slope earlier than the clastic regions of Svalbard and the Barents Sea.

The ice front was located inside Isfjorden after 12 ka (Mangerud et al., 1992). However, ice-rafting still dominated on the slope until approximately 9 ka (Figs. 13 and 17), suggesting that glaciers were grounded in the fjords of Svalbard and/or locally in the Barents Sea into the Early Holocene. Thus, the association between a light $\delta^{18}O$ peak and frequencies of IRD suggest that the final break-up of the Svalbard Ice Sheet started close to 12 ka and ended around 9 ka. The final disappearance of the ice sheet is associated with the lightest (2.58‰) $\delta^{18}O$ values.

The relatively high smectite accumulation that occurred during the late glacial/early Holocene period (~12–8 ka) may be related to increased sea ice production and/or sea ice-rafting from the Siberian shelf (Elverhøi et al., 1989) or from the Faeroe Islands (Kuhlemann et al., 1993), probably as a result of increased discharge of cold meltwater that cooled down the surface waters of the Norwegian–Greenland Sea.

During the early part of Holocene (~9–8 ka), bulk accumulation rates dropped to the present level. Since then, accumulation of hemipelagic mud has dominated on the slope, and ice-rafting has been generally low. In addition, the upper slope has been eroded by bottom currents, leaving a prominent lag deposit (Figs. 13 and 17).

8. Did the European and Laurentide ice sheets fluctuate coherently?

According to the established time scale of core NP90-39, there seems to be a certain temporal relationship between the IRD-rich sediments (*Heinrich* layers) deposited in the North Atlantic (Heinrich, 1988; Bond et al., 1992) and the clast-rich diamictons deposited on the western Svalbard slope (Fig. 17). The composition of these diamictons and similar deposits in the Norwegian–Greenland Sea (Wagner and Henrich, 1994) is different to those of the Heinrich layers in that they lack the specific limestone and dolomite grains derived from sources in eastern Canada (Bond et al., 1992). Therefore, the ice sheets covering north-western Europe and North America may have fluctuated synchronously on time scales shorter than the known orbital cycles. As IRD deposition occurs at the end of cooling cycles (Bond et al., 1993), they may be related to disintegration of the large ice sheets on the Northern Hemisphere.

However, IRD deposition on the western Svalbard slope (Fig. 17), in the Norwegian–Greenland Sea (Wagner and Henrich, 1994), and on the East Greenland margin (Nam et al., 1995; Stein et al., in press) occurred even at higher frequencies than the Heinrich events. In addition, the clast-rich diamictons off Svalbard were not deposited nearly instantaneously (within a few hundred years) as suggested for the Heinrich layers (Lehman, 1993). Instead, they were deposited over periods of 2000–5000 years (Fig. 17). These observations suggest that the marine-based Svalbard–Barents Sea Ice Sheet disintegrated more often than the Laurentide Ice Sheet, and it did not

collapse through surges as suggested for the Laurentide Ice Sheet (Bond et al., 1992). There seems to be a much closer relationship between the Svalbard–Barents Sea and the Fennoscandian ice sheets. This is first of all reflected by glaciation curves constructed for the Weichselian glaciation (Vorren et al., 1988; Mangerud, 1991; Mangerud and Svendsen, 1992; Elverhøi et al., 1993), but also by the temporal relationship between the onset of the last glacial melt in the Fram Strait (Jones and Keigwin, 1988) and the North Sea (Lehman and Keigwin, 1992), and the re-advance observed on the shelf off Svalbard, the shelf off Troms in northern Norway (Rokoengen et al., 1979), and in south-western Norway (Mangerud, 1977) between 13 and 12 ka.

We therefore speculate that the marine-based part of the Fennoscandian and Svalbard–Barents Sea ice sheets fluctuated more or less synchronously and therefore could have triggered the collapse of the Northern Hemisphere's ice sheets. This is in accordance with Jones and Keigwin (1988) who suggest, based on modelling studies by Peltier (1988a,b) and Nakada and Lambeck (1988), that marine down-draw of the marine-based Barents Sea Ice Sheet giving a sea-level rise of approximately 15 m could have triggered the decay of parts of the Laurentide Ice Sheet during the last glacial melt.

9. Conclusions

Five lithofacies groups have been defined on the western Svalbard continental slope. Laminated-to-layered mud and turbidites are supposed to reflect post-depositional reworking of the shelf banks caused by eustatic sea-level fall during ice-growth. Hemipelagic mud represents the background sediments and is evenly dispersed over the entire continental margin. Homogeneous and heterogeneous diamictons were deposited during glacial melt events (hemipelagic mud with IRD) and during peak glaciation on the submarine fans (debris flow deposits).

Hemipelagic mud with variable amounts of IRD was deposited during most of Isotope Stage 3 (59–27 ka). The ice-rafted debris deposited between 60 and 55 ka can be correlated with Glaciation E recorded at Kapp Ekholm. The glaciation was followed by three glacial advances. The composition and the frequency of the IRD suggests that the ice sheet was located in the eastern Svalbard–Barents Sea area at least until 44 ka, and that ice sheets at high northern latitudes fluctuated more frequently than previously thought.

The nucleation of the Late Weichselian Svalbard–Barents Sea Ice sheet was strengthened by an open-water lead established between the Fram Strait and the North Atlantic between 27 and 22.5 ka.

Eustatic lowering of the sea level during the ice growth led to bank exposure and erosion, bringing large amounts of fine-grained, organic-rich sediments to the deep-sea. As the ice sheet entered the continental shelf, soft sediments caused the ice to move rapidly to the shelf edge, producing a relatively thin ice.

The ice margin was located at the shelf edge at least between 19 and 14.5 ka. During peak glaciation, sedimentation was restricted to the submarine fans, and sediments were mainly transported downslope by debris flows.

The marine-based Svalbard–Barents Sea Ice Sheet started to retreat around 14.5 ka through massive iceberg discharge. The retreat was interrupted by a small and short-lived (13–12 ka) ice advance on the western Svalbard continental shelf, accompanied by erosion of the shelf banks and deposition of fine-grained organic-rich mud on the slope. The final ice recession started shortly after 12 ka, and was associated with a massive iceberg discharge from Svalbard. A comprehensive sea-ice cover was probably established during the final glacial melt, as a result of increased discharge of cold meltwater that cooled down the surface waters of the Norwegian–Greenland Sea. The frequencies of IRD suggests that the Barents Sea and the fjords of Svalbard became ice-free close to 9 ka.

Acknowledgments

This research was part of the Polar North Atlantic Margins, Late Cenozoic Evolution project

(PONAM). Financial support have been given by the University of Oslo and the Norwegian Polar Institute. Technical assistance was provided by Inger-Ann Hansen. Dierk Hebbeln, at the University of Bremen, has run the C/N ratio measurements, and Arnt Rørnes, at the University of Tromsø, did most of the petrographic determination. Victoria Cadman improved the English of the manuscript. The final version of the manuscript benefited from reviews provided by R. Stein and J. Sættem. This is contribution no. 301 of the Norwegian Polar Institute.

References

Aagaard, K., Swift, J.H. and Carmack, E.C., 1985. Thermohaline circulation in the Arctic Mediterranean Seas. J. Geophys. Res., 90: 4833–4846.

Aksu, A.E. and Piper, D.J.W., 1987. Late Quaternary sedimentation in Baffin Bay. Can. J. Earth Sci., 24: 1833–1846.

Alam, M., Piper, D.J.W. and Cooke, H.B.S., 1983. Late Quaternary stratigraphy and pale-oceanography of the Grand Banks continental margin, eastern Canada. Boreas, 12: 253–261.

Alm, T., 1993. Øvre Æråsvatn—palynostratigraphy of a 22,000 to 10,000 BP lacustrine record on Andøya, northern Norway. Boreas, 22: 171–188.

Andersen, E.S., Solheim, A. and Elverhøi, A., 1994. Development of a glaciated arctic continental margin: Exemplified by the western margin of Svalbard. In: D.K. Thurston and K. Fujita (Editors), Proc. Int. Conf. Arctic Margins, Anchorage, 1992 U.S. Dep. Inter. Miner. Manage. Serv., Alaska Outer Cont. Shelf Reg., OCS Study, MMS 94–0040, pp. 155–160.

Andersen, E.S., Østmo, S.R., Forsberg, C.F. and Lehman, S.J., 1995. Late- and post-glacial depositional environments in the Norwegian Trench, northern North Sea. Boreas, 24: 47–64.

Anderson, L.G., Jones, E.P., Lindegren, B., Rudels, B. and Sehlstedt, P.-I., 1988. Nutrient regeneration in cold, high salinity bottom water of the Arctic shelves. Cont. Shelf Res., 8: 1345–1355.

Berg, M.N., 1991. Sedimentologiske og geofysiske undersøkelser av sen-kenozoiske sedimenter på sydøstskråningen av Spitsbergenbanken, det nordlige Barentshav. Thesis. Univ. Oslo, 203 pp.

Bjørlykke, K., Bue, B. and Elverhøi, A., 1978. Quaternary sediments in the north western part of the Barents Sea and their relation to the underlying Mesozoic bedrock. Sedimentology, 25: 227–246.

Bjørlykke, K. and Elverhøi, A., 1975. Reworking of Mesozoic clayey material in the north-western part of the Barents Sea. Mar. Geol., 18: M29–M34.

Boles, J.R. and Franks, S.G., 1979. Clay diagenesis in Wilcox sandstones of Southeast Texas: implications of smectite diagenesis in sandstone cementation. J. Sediment. Petrol., 49: 55–70.

Bond, G., Broecker, W., Johnsen, S., McManus, J., Labeyrie, L., Jouzel, J. and Bonani, G., 1993. Correlations between climate records from North Atlantic sediments and Greenland ice. Nature, 365: 143–147.

Bond, G., Heinrich, H., Broecker, W., Labeyrie, L., McManus, J., Andrews, J., Huon, S., Jantschik, R., Clasen, S., Simet, C., Tedesco, K., Klas, M., Bonani, G. and Ivy, S., 1992. Evidence for massive discharges of icebergs into the North Atlantic ocean during the last glacial period. Nature, 360: 245–249.

Boulton, G.S., 1990. Sedimentary and sea level changes during glacial cycles and their control of glacimarine facies architecture. In: J.A. Dowdeswell and J.D. Scourse (Editors), Glacimarine Environments: Processes and Sediments. Geol. Soc. Spec. Publ., 53: 15–52.

Bouma, A.H., 1962. Sedimentology of some Flysch Deposits. Elsevier, Amsterdam, 168 pp.

Chough, S.K. and Hesse, R., 1985. Contourites from Eirik Ridge, south of Greenland. Sediment. Geol., 41: 185–199.

Clayton, L., Mickelson, D.M. and Attig, J.W., 1989. Evidence against pervasively deformed bed material beneath rapidly moving lobes of the southern Laurentide Ice Sheet. Sediment. Geol., 62: 203–208.

Clayton, L., Teller, J.T. and Attig, J.W., 1985. Surging of the south-western part of the Laurentide Ice Sheet. Boreas, 14: 235–241.

Crane, K. and Solheim, A., 1995. Seafloor atlas of the northern Norwegian–Greenland Sea. Nor. Polarinst. Medd., 137.

Dokken, T.M., 1995. Paleoceanographic changes during the last interglacial–glacial cycle from the Svalbard-Barents Sea margin: Implications for ice growth and decay. Thesis. Univ. Tromsø.

Ehrmann, W.U., Melles, M., Kuhn, G. and Grobe, H., 1992. Significance of clay mineral assemblages in the Antarctic Ocean. Mar. Geol., 107: 249–273.

Elverhøi, A., 1979. Sedimentological and mineralogical investigations of Quaternary bottom sediments off the Norwegian west coast. Nor. Geol. Tidsskr., 59: 273–284.

Elverhøi, A., Andersen, E.S., Dokken, T., Hebbeln, D., Spielhagen, R., Svendsen, J.I., Sørflaten, M., Rørnes, A., Hald, M. and Forsberg, C.F., 1995a. The growth and decay of the Late Weichselian Ice Sheet in western Svalbard and adjacent areas based on provenance studies of marine sediments. Quat. Res., 44: 303–316.

Elverhøi, A., Fjeldskaar, W., Solheim, A., Nyland-Berg, M. and Russwurm, L., 1993. The Barents sea—A model of its growth and decay during the last ice maximum. Quat. Sci. Rev., 12: 863–873.

Elverhøi, A. and Grønlie, G., 1981. Diagenetic and sedimentologic explanation for high seismic velocity and low porosity in Mesozoic–Tertiary sediments, Svalbard Region. Bull. AAPG, 65: 145–153.

Elverhøi, A., Pfirman, S.L., Solheim, A. and Larssen, B.B., 1989. Glaciomarine sedimentation in epicontinental seas exemplified by the northern Barents Sea. Mar. Geol., 85: 225–250.

Elverhøi, A., Svendsen, J.I., Solheim, A., Andersen, E.S., Milliman, J., Mangerud, J. and Hooke, R. LeB., 1995b. Late Quaternary sediment yield from the High Arctic Svalbard area. J. Geol., 103: 1–17.

Fairbanks, R.G., 1989. A 17,000-year glacio-eustatic sea level record: influence of glacial melting rates on the Younger Dryas event and deep-ocean circulation. Nature, 342: 637–642.

Fillon, R.H., Miller, G.H. and Andrews, J.T., 1981. Terrigenous sand in Labrador Sea hemipelagic sediments and paleoglacial events on Baffin Island over the last 100,000 years. Boreas, 10: 107–124.

Foldvik, A. and Gammelsrød, T., 1988. Notes on Southern Ocean hydrography, sea-ice and bottom water formation. Palaeogeogr. Palaeoclimatol. Palaeoecol., 67: 3–17.

Folk, R.L. and Ward, W.C., 1957. Brazoa River Bar: a study in the significance of grain size parameters. J. Sediment. Petrol., 27: 23–26.

Forsberg, C.F., 1983. Sedimentological and early diagenetic studies in the Barents Sea. Thesis. Univ. Oslo, 120 pp.

Frey, R.W. and Pemberton, S.G., 1984. Trace fossil facies models. In: R.G. Walker (Editor), Facies Models. Geosci. Can. Reprint Ser. 1, 2nd ed., pp. 189–207.

Gonthier, E.G., Faugères, J.-C. and Stow, D.A.V., 1984. Contourite facies of the Faro Drift, Gulf of Cadiz. In: D.A.V. Stow and D.J.W. Piper (Editors), Fine-Grained Sediments Deep-water Processes and Facies. Geol. Soc. London Spec. Publ., 15: 275–292.

Haake, F.-W. and Pflaumann, U., 1989. Late Pleistocene foraminiferal stratigraphy on the Vøring Plateau, Norwegian Sea. Boreas, 18: 343–356.

Hancock, J.M., 1984. Cretaceous. In: K.W. Glennie (Editor), Introduction to the Petroleum Geology of the North Sea. Blackwell, Oxford, pp. 133–150.

Hebbeln, D., 1992. Weichselian glacial history of the Svalbard area: Correlation the marine and terrestrial record. Boreas, 21: 295–304.

Hebbeln, D., Dokken, T., Andersen, E.S., Hald, M. and Elverhøi, A., 1994. Moisture supply for northern ice-sheet growth during the Last Glacial Maximum. Nature, 350: 409–411.

Heinrich, H., 1988. Origin and consequences of cyclic ice rafting in the north-east Atlantic Ocean during the past 130,000 years. Quat. Res., 29: 143–152.

Henrich, R. and Baumann, K.-H., 1994. Evolution of the Norwegian current and the Scandinavian Ice Sheets during the past 2.6 m.y.: evidence from ODP Leg 104 biogenic carbonate and terrigenous records. Palaeogeogr. Palaeoclimatol. Palaeoecol., 108: 75–94.

Henrich, R., Kassen, H., Vogelsang, E. and Thiede, J., 1989. Sedimentary facies of glacial–interglacial cycles in the Norwegian Sea during the last 350 ka. Mar. Geol., 86: 283–319.

Hower, J., Eslinger, E.V., Hower, M.E. and Perry, E.A., 1976. Mechanism of burial metamorphism of argillaceous sediments: 1. Mineralogical and chemical evidence. Geol. Soc. Am. Bull., 87: 725–737.

Hurlbut Jr., C.S. and Klein, C., 1977. Manual of Mineralogy. Wiley, New York, 19th ed., 532 pp.

Jones, G.A. and Keigwin, L.D., 1988. Evidence from Fram Strait (78 °N) for early deglaciation. Nature, 336: 56–59.

Kuhlemann, J., Lange, H. and Paetsch, H., 1993. Implications of a connection between clay mineral variations and coarse grained debris and lithology in the central Norwegian–Greenland Sea. Mar. Geol., 114: 1–11.

Laberg, J.S., 1994. Late Pleistocene evolution of the submarine fans off western Barents Sea margin. Thesis. Univ. Tromsø.

Landvik, J., Bolstad, M., Lycke, A.K., Mangerud, J. and Sejrup, H.P., 1992. Weichselian stratigraphy and palaeoenvironments at Bellsund, western Svalbard. Boreas, 21: 335–358.

Lehman, S.J., 1993. Ice sheets, wayward winds and sea change. Nature, 365: 108–110.

Lehman, S.J. and Keigwin, L.D., 1992. Sudden changes in North Atlantic circulation during the last deglaciation. Nature, 356: 757–762.

Mangerud, J., 1977. Late Weichselian marine sediments containing shells, foraminifera and pollen, at Ågotnes, Western Norway. Nor. Geol. Tidsskr., 57: 21–54.

Mangerud, J., 1991. The last interglacial/glacial cycle in northern Europe. In: L.C.K. Shane and E.J. Cushing (Editors), Quaternary Landscapes. Univ. Minnesota Press, Minneapolis, pp. 38–75.

Mangerud, J., Bolstad, M., Elgersma, A., Helliksen, D., Landvik, J.Y., Lønne, I., Lycke, A.K., Salvigsen, O., Sandhal, T. and Svendsen, J.I., 1992. The last glacial maximum on Spitsbergen, Svalbard. Quat. Res., 38: 1–31.

Mangerud, J. and Gulliksen, S., 1975. Apparent radiocarbon age of recent marine shells from Norway, Svalbard and Ellesmere Island. Quat. Res., 5: 263–273.

Mangerud, J. and Svendsen, J.I., 1992. The last interglacial–glacial period on Spitsbergen, Svalbard. Quat. Sci. Rev., 11: 633–664.

Manum, S.B. and Throndsen, T., 1978. Rank of coal and dispersed organic matter and its geological bearings on the Spitsbergen Tertiary. Nor. Polarinst. Årbok, 1977: 159–177.

Micromeritics, 1978. Instruction manual: SediGraph Particle Size Analyser.

Miller, G.H., Sejrup, H.P., Lehman, S.J. and Forman, S.L., 1989. Glacial history and marine environmental change during the last interglacial–glacial cycle, western Spitsbergen, Svalbard. Boreas, 18: 273–296.

Nakada, M. and Lambeck, K., 1988. The melting history of the last Pleistocene Antarctic ice sheet. Nature, 333: 36–40.

Nam, S.-I., Stein, R., Grobe, H. and Hubberten, H., 1995. Late Quaternary glacial–interglacial changes in sediment composition at the East Greenland continental margin and their paleoceanographic implications. Mar. Geol., 122: 243–262.

Paterson, W.S.B., 1994. The Physics of Glaciers. Pergamon, 3rd ed., 480 pp.

Pearson, M.J., 1990. Clay mineral distribution and provenance in Mesozoic and Tertiary mudrocks of the Moray Firth and northern North Sea. Clay Miner., 25: 519–541.

Pearson, M.J. and Small, J.S., 1988. Illite–smectite diagenesis and palaeotemperatures in northern North Sea Quaternary to Mesozoic shale sequences. Clay Miner., 23: 109–132.

Peltier, W.R., 1988a. Global sea level and earth rotation. Science, 240: 895–901.

Peltier, W.R., 1988b. Lithospheric thickness, Antarctic deglaciation history, and ocean basin discretization effects in a global model of postglacial sea level change: a summary of some sources of nonuniqueness. Quat. Res., 29: 93–112.

Peters, K.E., 1986. Guidelines for evaluating petroleum source rock using programmed pyrolysis. AAPG Bull., 70: 318–329.

Polyak, L., Lehman, S.J., Gataullin, V. and Jull, A.J.T., 1995. Two-step deglaciation of the southeastern Barents Sea. Geology, 23: 567–571.

Quadfasel, D., Rudels, B. and Kurz, K., 1988. Outflow of dense water from a Svalbard fjord into the Fram Strait. Deep-Sea Res., 35: 1143–1150.

Reynolds Jr., R.C. and Hower, J., 1970. The nature of interlayering in mixed-layer illite montmorillonites. Clays Clay Miner., 18: 25–36.

Rokoengen, K., Bugge, T. and Løfaldli, M., 1979. Quaternary geology and deglaciation of the continental shelf off Troms, north Norway. Boreas, 8: 217–227.

Ruddiman, W.F. and McIntyre, A., 1976. Northeast Atlantic paleoclimatic changes over the past 600,000 years. Geol. Soc. Am. Mem., 145: 111–146.

Rundberg, Y., 1989. Tertiary sedimentary history and basin evolution of the Norwegian North Sea between 60°–62°N—an integrated approach. Thesis. Univ. Trondheim.

Schültz, L.G., 1964. Quantitative interpretation of mineralogical composition from X-ray and chemical data for the Pierre Shale. Analytical methods in geochemical investigations of the Pierre Shale. Geol. Surv. Prof. Pap., 391-C: 1–31.

Sejrup, H.P., Haflidason, H., Aarseth, I., King, E., Forsberg, C.F., Long, D. and Rokoengen, K., 1994. Late Weichselian glaciation history of the northern North Sea. Boreas, 23: 1–13.

Shanmugam, G. and Moiola, R.J., 1982. Eustatic control of turbidites and winnowed turbidites. Geology, 10: 231–235.

Siegert, M.J. and Dowdeswell, J.A., 1995. Modelling ice sheet sensitivity to Late Weichselian environment in the Svalbard–Barents Sea region. J. Quat. Sci., 10: 33–43.

Sigmond, E.M.O., 1992. Bedrock map of Norway and adjacent ocean areas. Scale 1:3 million. Geol. Surv. Norway.

Solheim, A., 1991. The depositional environment of surging sub-polar tidewater glaciers: A case study of the morphology, sedimentation and sediment properties in a surge-affected marine basin outside Nordaustlandet, northern Barents Sea. Nor. Polarinst. Skr., 194, 97 pp.

Solheim, A., Elverhøi, A., Andersen, E.S. and Jahre, H., 1991. Marine geological/geophysical cruise on the western Svalbard margin 1990, cruise report. Nor. Polarinst. Rapportser., 69, 96 pp.

Solheim, A., Milliman, J. and Elverhøi, A., 1988. Sediment distribution and sea floor morphology of Storbanken: Implications for the glacial history of the northern Barents Sea. Can. J. Earth Sci., 25: 547–556.

Spielhagen, R., 1991. Die Eisdrift in der Fram Strasse während der letzen 200,000 Jahre. Geomar Rep., 4: 1–144.

Stein, R., 1985. Rapid grain-size analyses of clay and silt fraction by SediGraph 5000D: Comparison with coulter counter and Atterberg methods. J. Sediment. Petrol., 55: 590–615.

Stein, R., Grobe, H. and Wahsner, M., 1994a. Organic carbon, carbonate, and clay mineral distributions in eastern central Arctic Ocean surface sediments. Mar. Geol., 119: 269–285.

Stein, R., Nam, S.-I., Grobe, H. and Hubberten, H., in press. Late Quaternary glacial history and short-term IRD fluctuations along the East Greenland continental margin. In: J. Andrews et al. (Editors), Late Pleistocene North Atlantic Paleoceanography. Geol. Soc. London Spec. Publ.

Stein, R., Nam, S.-I., Schubert, C., Vogt, C., Fütterer, D. and Heinemeier, J., 1994b. The last deglaciation in the Eastern Central Arctic Ocean. Science, 264: 692–696.

Stevenson, F.J. and Cheng, C.-N., 1972. Organic geochemistry of the Argentine Basin sediments: carbon-nitrogen relationships and Quaternary correlations. Geochim. Cosmochim. Acta, 36: 653–671.

Stow, D.A.V., 1979. Distinguishing between fine-grained turbidites and contourites on the Nova Scotian deep water margin. Sedimentology, 26: 371–387.

Stow, D.A.V., 1985. Fine-grained sediments in deep-water: An overview of processes and facies models. Geo-Mar. Lett., 5: 17–23.

Stow, D.A.V. and Holbrook, J.A., 1984. North Atlantic contourites: an overview. In: D.A.V. Stow and D.J.W. Piper (Editors), Fine-Grained Sediments Deep-water Processes and Facies. Geol. Soc. London Spec. Publ., 15: 245–256.

Stow, D.A.V. and Piper, D.J.W., 1984. Deep-water fine-grained sediments: facies models. In: D.A.V. Stow and D.J.W. Piper (Editors), Fine-Grained Sediments Deep-water Processes and Facies. Geol. Soc. London Spec. Publ., 15: 611–645.

Svendsen, J.I., Mangerud, J., Elverhøi, A., Solheim, A. and Schüttenhelm, R.T.E., 1992. The Late Weichselian glacial maximum on western Spitsbergen inferred from offshore sediment cores. Mar. Geol., 104: 1–17.

Sættem, J., Poole, D.A.R., Ellingsen, L. and Sejrup, H.P., 1992. Glacial geology of outer Bjørnøyrenna, southwestern Barents Sea. Mar. Geol., 103: 15–51.

Sørflaten, M., 1993. Siste interglasiale/glasiale syklus på Svalbards vestmargin basert på utbredelse og sammensetning av isdroppet materiale. Thesis. Univ. Oslo, 224 pp.

Vogt, P., Sundvor, E., Crane, C., Pfirman, S., Nishimura, C. and Max, M., 1990. SeaMARCII and associated geophysical investigation of the Knipovich Ridge, Molloy Ridge/Fracture Zone, and Barents Spitsbergen continental margin. 3. Sedimentary processes. EOS, 71(17)(abstr.).

Vorren, T.O., Vorren, K.-D., Alm, T., Gulliksen, S. and Løvlie, R., 1988. The last deglaciation (20.000–11.000 B.P.) on Andøya, northern Norway. Boreas, 17; 41–77.

Wagner, T. and Henrich, R., 1994. Organo- and lithofacies of glacial/interglacial deposits in the Norwegian–Greenland Sea: responses to paleoceanographic and paleoclimatic changes. Mar. Geol., 120: 335–364.

Wright, R. and Anderson, J.B., 1982. The importance of sediment gravity flow to sediment transport and sorting in a glacial marine environment: Eastern Weddell Sea, Antarctica. Geol. Soc. Am. Bull., 93: 951–963.

Yoon, S.H., Chough, S.K., Thiede, J. and Werner, F., 1991. Late Pleistocene sedimentation on the Norwegian continental slope between 67° and 71°N. Mar. Geol., 99: 187–207.